ARTICLE

The budding yeast RSC complex maintains ploidy by promoting spindle pole body insertion

Tina L. Sing[1,2] ⓘ, Minnie P. Hung[1,2] ⓘ, Shinsuke Ohnuki[3] ⓘ, Godai Suzuki[3], Bryan-Joseph San Luis[2,4], Melainia McClain[5], Jay R. Unruh[5] ⓘ, Zulin Yu[5], Jiongwen Ou[1,2], Jesse Marshall-Sheppard[1,2] ⓘ, Won-Ki Huh[6] ⓘ, Michael Costanzo[2,4] ⓘ, Charles Boone[2,4], Yoshikazu Ohya[3], Sue L. Jaspersen[5,7] ⓘ, and Grant W. Brown[1,2] ⓘ

Ploidy is tightly regulated in eukaryotic cells and is critical for cell function and survival. Cells coordinate multiple pathways to ensure replicated DNA is segregated accurately to prevent abnormal changes in chromosome number. In this study, we characterize an unanticipated role for the *Saccharomyces cerevisiae* "remodels the structure of chromatin" (RSC) complex in ploidy maintenance. We show that deletion of any of six nonessential RSC genes causes a rapid transition from haploid to diploid DNA content because of nondisjunction events. Diploidization is accompanied by diagnostic changes in cell morphology and is stably maintained without further ploidy increases. We find that RSC promotes chromosome segregation by facilitating spindle pole body (SPB) duplication. More specifically, RSC plays a role in distributing two SPB insertion factors, Nbp1 and Ndc1, to the new SPB. Thus, we provide insight into a role for a SWI/SNF family complex in SPB duplication and ploidy maintenance.

Introduction

Ploidy is defined by the number of complete sets of chromosomes in an organism. Human cells generally maintain the diploid state; however, controlled changes in ploidy levels are required for processes such as gametogenesis, cellular development, and differentiation. In contrast, unscheduled changes in ploidy can lead to genome instability and aneuploidy, both of which contribute to disease (Davoli and de Lange, 2011). Additionally, ploidy alterations in pathogenic organisms can lead to evolved drug resistance (Harrison et al., 2014) or cellular growth that allows for evasion of the host's immune system (Zaragoza et al., 2010; Okagaki and Nielsen, 2012). Thus, defining the pathways that maintain ploidy, as well as the consequences of changing ploidy states, is critical to understand diverse aspects of cell function.

Cellular pathways that are important for ploidy control include those involved in DNA replication, chromosome segregation, and cytokinesis. Studies in *Saccharomyces cerevisiae* have led to the identification and characterization of proteins involved in ploidy maintenance, particularly proteins involved in duplicating the spindle pole body (SPB), which is the yeast centrosome (Schild et al., 1981; Winey et al., 1991; Chial et al., 1999; Jaspersen et al., 2002). The SPB is a large protein complex that is embedded in the nuclear envelope and is duplicated once per cell cycle (Jaspersen and Winey, 2004; Winey and Bloom, 2012). Thus, one critical step of SPB duplication is the insertion of the newly duplicated SPB into the nuclear envelope. Several key SPB insertion factors (Bbp1, Mps2, Mps3, Nbp1, and Ndc1) have been characterized, but the exact mechanism of how insertion is achieved remains elusive (Winey et al., 1991, 1993; Schramm et al., 2000; Jaspersen et al., 2002; Araki et al., 2006; Rüthnick et al., 2017). SPB insertion is thought to involve the nuclear pore complex (NPC), a nuclear membrane-spanning complex that is responsible for nuclear import and export. Many studies suggest that Ndc1, a shared component of the SPB and NPC, is involved in creating an opening in the nuclear envelope that is necessary for protein complex insertion (Chial et al., 1999; Sezen et al., 2009; Witkin et al., 2010; Chen et al., 2014; Katta et al., 2015; Sezen, 2015; Rüthnick et al., 2017). In support of this idea, Ndc1 mutants are unable to properly insert either the SPB or the NPC into the nuclear envelope (Lau et al., 2004; Onischenko et al., 2009). Interestingly, appropriate expression of Ndc1 is critical for SPB insertion, where having too much or too little Ndc1 causes SPB insertion defects (Chial et al., 1999).

SPB insertion also relies on the nuclear import of the Ndc1-binding partner, Nbp1 (Araki et al., 2006; Kupke et al., 2011;

[1]Department of Biochemistry, University of Toronto, Toronto, Ontario, Canada; [2]Donnelly Centre for Cellular and Biomolecular Research, University of Toronto, Toronto, Ontario, Canada; [3]Department of Integrated Biosciences, Graduate School of Frontier Sciences, University of Tokyo, Chiba, Japan; [4]Department of Molecular Genetics, University of Toronto, Toronto, Ontario, Canada; [5]Stowers Institute for Medical Research, Kansas City, MO; [6]Department of Biological Sciences, Seoul National University, Seoul, Republic of Korea; [7]Department of Molecular and Integrative Physiology, University of Kansas Medical Centre, Kansas City, KS.

Correspondence to Grant W. Brown: grant.brown@utoronto.ca.

Rüthnick et al., 2017). After translation in the cytoplasm, the karyopherin Kap123 binds the bipartite nuclear localization signal 1 (NLS1) of Nbp1 leading to transportation to the NPC (Kupke et al., 2011). Nuclear import through the NPC releases Nbp1 from Kap123, which exposes the amphipathic α helix on Nbp1, causing binding to the nuclear envelope. Nbp1 then localizes to the SPB where it helps mediate insertion of the new SPB into the nuclear envelope. Interestingly, deletion of *KAP123* has been shown to cause spontaneous diploidization (Ptak et al., 2009), which corresponds to an accumulation of Nbp1 in the cytoplasm (Kupke et al., 2011). Data suggest that timely localization of Nbp1 to the nuclear side of the duplicating SPB is critical for SPB insertion into the nuclear envelope (Burns et al., 2015).

The diversity of pathways that could impinge on ploidy maintenance by influencing SPB function has not been probed systematically. Recently, chromatin remodeling complexes have been implicated in ploidy maintenance in yeast (Lanzuolo et al., 2001; Yu et al., 2006; Campsteijn et al., 2007; Chambers et al., 2012; Wang and Cheng, 2012; Imamura et al., 2015) and higher eukaryotes (Isakoff et al., 2005; Vries et al., 2005; Sillibourne et al., 2007). In this study, we find that the yeast "remodels the structure of chromatin" (RSC) complex is a key element in maintaining chromosome number and reveal an unanticipated role for RSC in promoting SPB insertion into the nuclear envelope. RSC is a 17-subunit SWI/SNF family chromatin remodeler that has diverse functions in regulating gene expression in chromatin transactions (Laurent et al., 1992; Cairns et al., 1996, 1998, 1999; Cao et al., 1997; Angus-Hill et al., 2001; Romeo et al., 2002; Sanders et al., 2002; Baetz et al., 2004). We show that six of seven nonessential RSC subunits facilitate SPB insertion in a transcription-independent manner. More specifically, we find that the RSC subunit Htl1 is required for proper distribution of the insertion factors Nbp1 and Ndc1 to the duplicating SPB.

Results

Nonessential *RSC* genes maintain ploidy

The budding yeast nonessential gene deletion collection is an important resource for the functional dissection of the eukaryotic cell (Giaever and Nislow, 2014). We found that haploid deletion mutants of nonessential *RSC* subunit genes had become diploid over time. As some connections between *RSC* genes and gains in ploidy have been noted (Romeo et al., 2002; Yu et al., 2006; Campsteijn et al., 2007; Wang and Cheng, 2012; Imamura et al., 2015), we developed an assay for detecting ploidy increases, generating fresh haploid deletion mutants of the seven nonessential *RSC* genes by sporulating heterozygotes and monitoring DNA content during 100 generations of growth (Fig. 1 a). Deletion of *RSC1*, *RSC2*, *RSC30*, *LDB7*, *NPL6*, or *HTL1*, but not *RTT102*, caused haploid cells to spontaneously diploidize after germination (Fig. 1 b). Biological replicates of this assay showed that each *rscΔ* strain diploidized after a characteristic number of generations, suggesting that individual subunits play unequal roles in ploidy maintenance. The diploidization rate of each deletion mutant remained consistent between replicates despite differences in mating type or auxotrophic markers. Comparative genome hybridization (CGH) on tiling microarrays revealed that diploidized *rscΔ* strains acquired two complete copies of the genome and were not aneuploid (Fig. S1 a). We were unable to detect mating-type switches in diploidized strains, indicating that the ploidy increases occurred through autodiploidization (Figs. 1 c and S1, b and c).

In all cases, *rscΔ* mutants propagated stably as diploids, without evidence of tetraploidization. To gain insight into how diploids arise rapidly without subsequent ploidy gain to produce tetraploids, we compared the growth rates of *rscΔ* haploids to *rscΔ* diploids (Figs. 1 d and S1 d). In all testable cases, diploidization caused only a modest decrease in doubling time compared with the haploid counterpart, suggesting that the rapid diploidization must be due to frequent diploidization events rather than a rare event accompanied by a large fitness gain. Because *rscΔ* tetraploids are not detectable during 100 generations of growth, we created tetraploid *rscΔ* cells by mating diploidized *MAT**a**/a* and *MATα/α* strains to make *MAT**a**/**a**/α/α* homozygous *rscΔ* tetraploid strains. We then compared the viability of the tetraploids to that of the haploid and diploid *rscΔ* cells (Fig. 1, e and f). In the wild-type strains, no dead cells were detected after 20 generations in haploid and diploid populations, whereas the tetraploid population showed a slight reduction in viability (Fig. 1 e). The *rsc2Δ* strains showed decreased viability compared with the wild-type control, but little effect of ploidy on viability. In contrast, the *htl1Δ* tetraploids showed a clear decrease in viability (Fig. 1 e). Flow cytometric analysis indicated that the *rsc2Δ* tetraploid population reverted back to diploid, suggesting a ploidy drive to the diploid state (Fig. 1 f). The *htl1Δ* tetraploids showed evidence of aneuploidy (Fig. 1 f). Together, these data suggest that tetraploids are not detected in *rscΔ* populations because these cells either revert back to the diploid state (as in *rsc2Δ*) or become inviable because of aneuploidy (as in *htl1Δ*).

Distinct morphological features define diploidized *rscΔ* mutants

To evaluate the effect of spontaneous diploidization on cell morphology, we measured 254 cellular features of *rscΔ* mutants using CalMorph software (Ohya et al., 2005). The two most obvious features that differentiated diploidized *rscΔ* mutants from the haploid wild type, *rtt102Δ*, or the majority of the deletion collection were the whole-cell size in budded cells that contain only one nucleus (C101_A1B) and the bud–axis ratio in budded cells that contain only one nucleus (C114_A1B; Fig. 2 a). Identification of these features was consistent with the relationship between increasing ploidy and cell size (Otto, 2007) and with the elongated bud phenotype documented in *rscΔ* mutants (Watanabe et al., 2009).

Principal component analysis (PCA) was used to visualize morphological features that distinguished diploidized *rscΔ* mutants. As a control, we found that *rtt102Δ* is morphologically similar to *MAT**a*** wild-type haploids, whereas diploidized *rscΔ* strains are morphologically distinct from *MAT**a*** wild-type haploids and *MAT**a**/α* wild-type diploids (Fig. 2 b) but similar to wild-type *MAT**a**/**a*** diploids. Thus, morphological analysis suggests that *rscΔ* mutants diploidize by an autodiploidization event rather than cellular fusion of two cells by mating, consistent with the mating-type analysis (Fig. 1 c). We extracted 120 measurements that contributed most strongly to the variance detected by PCA and used hierarchical clustering analysis to identify 10
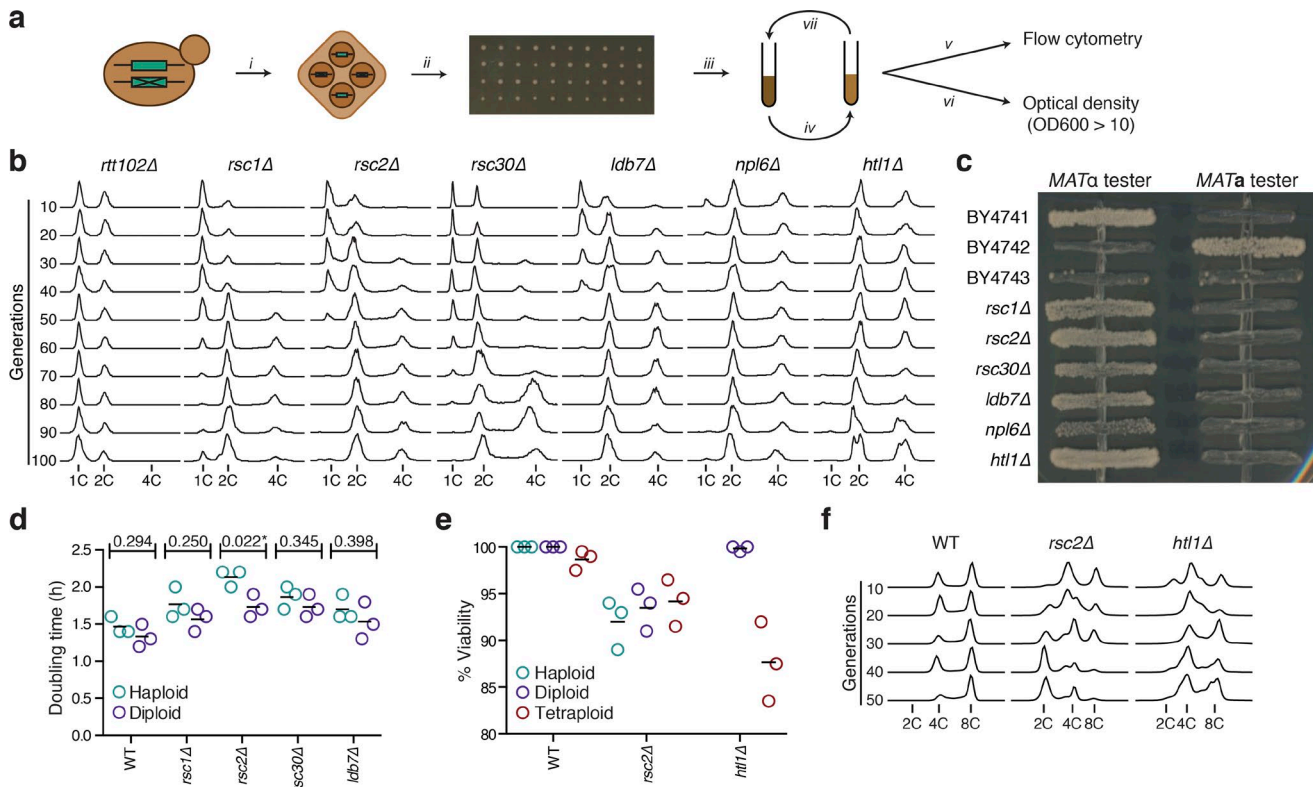
Figure 1. **Haploid *RSC* deletion mutants spontaneously form stable diploids. (a)** Heterozygous *rscΔ* strains were sporulated (i) and dissected (ii). A resulting colony was used to inoculate a liquid culture (iii), which was grown to saturation (iv). Saturated cultures were diluted and grown for an additional 4 h and then fixed for flow cytometry (v), and the OD_{600} of the saturated culture was measured (vi). The saturated culture was then diluted 1 in 1,000 (vii) to repeat steps iv to vii for 10 cycles, which represents ~100 generations of growth. **(b)** Flow cytometric analysis of samples taken from panel a for the indicated strains. Histograms represent the distributions of ~10,000 cells after growth for the indicated number of generations after germination. Positions of cells with 1C, 2C, and 4C DNA content are indicated on the x axis, which reflects fluorescence intensity on a linear scale. The y axis of each graph, which represents cell frequency, has been scaled to represent the percentage of the maximum bin contained in that graph. **(c)** Diploidized *rscΔ* strains were subjected to a mating-type test with a *MATa* and a *MATα* strain. Growth on minimal medium signifies a mating event. Wild-type *MATa* (BY4741), *MATα* (BY4742), and *MATa/α* (BY4743) strains were included as controls. **(d)** The maximum doubling time was calculated from growth curves depicted in Fig. S1 d for three technical replicates. The P values from a one-sided Student's *t* test are shown. Data distributions were assumed to be normal, but were not formally tested. Black bars represent the means. **(e)** Viability was assessed using methylene blue staining of logarithmically grown cells for three technical replicates. Haploids and diploids represent cells grown for 10 and 100 generations after germination. Tetraploids were obtained by mating diploidized cells. At least 200 cells were scored as alive (white) or dead (blue), and the percentage of viable cells is indicated. Black bars indicate the means. The *htl1Δ* strain cannot be maintained as a haploid. **(f)** Ploidy of the indicated tetraploid strains was monitored by flow cytometry as in panel b, except the x-axis is on a logarithmic scale.

representative traits that define diploidized *rscΔ* morphology (Table S1). We anticipate that these features may be indicative of spontaneous ploidy increase and could be used to find new ploidy maintenance genes in future studies.

To test if the effect of losing nonessential RSC subunits was characteristic of loss of RSC function in general, we analyzed the morphology of conditional mutants in the catalytic subunit of RSC, Sth1 (Fig. 2, c and d). We found that *sth1-2*, but not *sth1-3*, was morphologically similar to the diploidized *rscΔ* mutants and to *MATa/a* cells and that *sth1-2*, but not *sth1-3*, had diploidized. Together, these data demonstrate that both nonessential and essential RSC subunits maintain ploidy and define a set of morphological features that are specific to *MATa/a* diploids.

SPB duplication is defective in *rsc* mutants

The spontaneous diploidization observed in *rscΔ* mutants is reminiscent of mutants with defective SPB duplication that missegregate a complete chromosome set (Schild et al., 1981; Winey et al., 1991, 1993; Chial et al., 1999; Schramm et al., 2000;

Jaspersen et al., 2002; Araki et al., 2006). To assess SPB function, fresh haploid cells containing an *rscΔ*, mCherry-tagged histone H2A and GFP-tagged Spc42 were grown to mid-logarithmic phase, and defective SPBs in large-budded cells were quantified (Fig. 3 a). The total number of SPB defects in diploidizing *rscΔ* strains increased dramatically relative to the haploid wild-type and the *rtt102Δ* strain. Monopolar SPBs (where only a single SPB is detected), dead SPBs (where the DNA mass marked by histone-mCherry fails to associate with one of the SPBs), and multiple SPBs were markedly increased in all of the diploidizing *rscΔ* strains. We infer that the ploidy gain in *rscΔ* mutants is due to SPB defects that result in segregation failures. Consistent with distinct roles for each subunit in the ploidy maintenance function of RSC, the individual mutants showed distinct patterns and numbers of SPB defects, although our evidence (below) points to a common origin for the distinct SPB defects. We were surprised that the total number of SPB defects did not correlate with the rate of spontaneous diploidization observed by flow cytometry (Fig. 1 b); however, kinetic studies (below) revealed that assessing
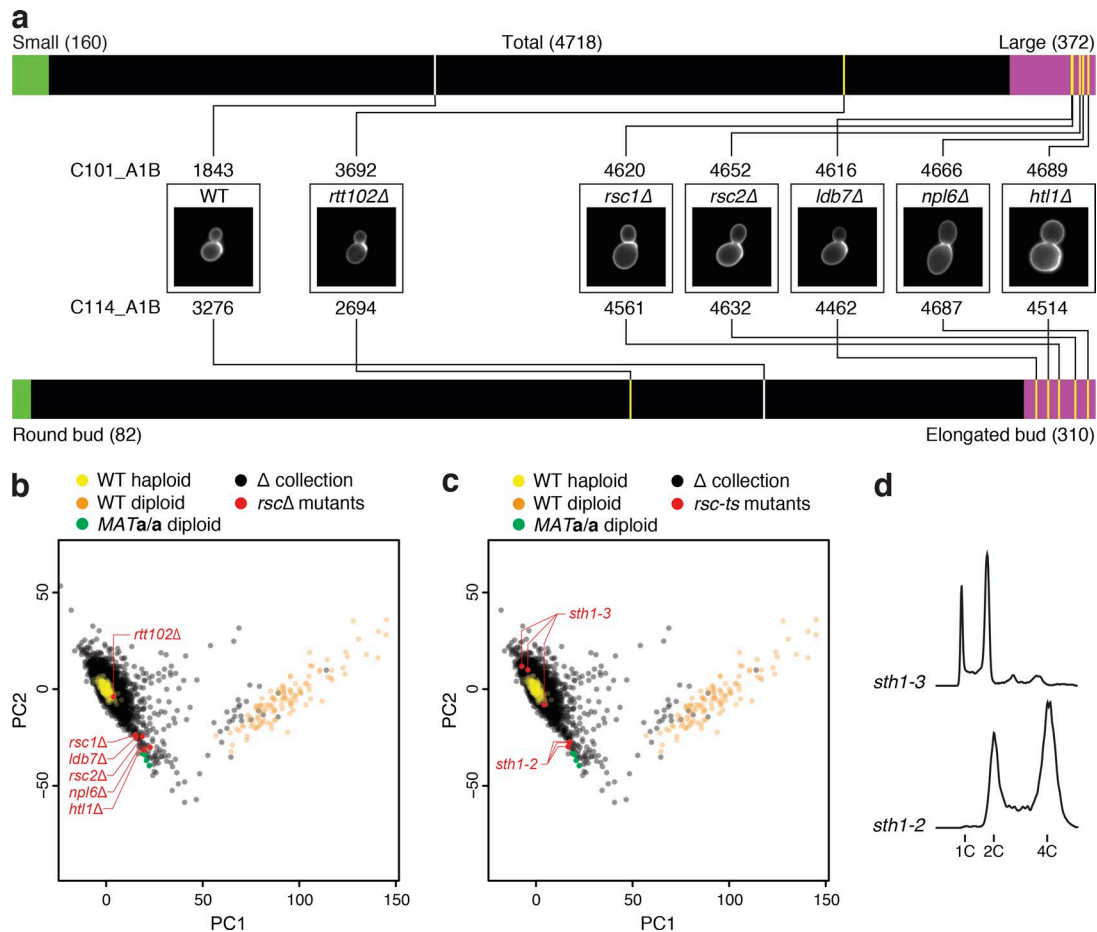
Figure 2. Diploidized *rscΔ* mutants are morphologically distinct from wild-type *MATa/α* diploids. (a) CalMorph software was used to analyze the yeast deletion collection. Strains were ranked by whole-cell size in budded cells containing one nucleus (C101_A1B) or by bud/axis ratio in budded cells containing one nucleus (C114_A1B) and displayed graphically. Mutants that are smaller (top) or have rounder buds (bottom) than wild type are shown in green. Mutants that are larger (top) or have more elongated buds (bottom) than wild type are shown in pink. The haploid wild-type strain is shown in white, and the *rscΔ* mutants are shown in yellow. Representative images of wild-type and *rscΔ* cells are shown. The number above or below the image represents the rank number among the 4,718 deletion mutants analyzed for C101_A1B or C114_A1B, respectively. **(b)** PCA was applied to the morphological dataset created for the haploid yeast deletion collection. **(c)** Strains with temperature-sensitive alleles of *STH1* were imaged and analyzed with CalMorph and plotted in the context of the analysis in panel b. **(d)** The DNA contents of the indicated strains after 24 h of logarithmic growth at 23°C are plotted.

SPB function by analyzing static images can result in a high false-negative rate. Finally, most diploidizing *rscΔ* mutants had increased instances of multiple SPBs, a phenotype only rarely seen in the INO80 mutant, *ies6Δ*, which also spontaneously diploidizes (Fig. S2 a; Chambers et al., 2012). We suggest that the RSC and INO80 chromatin remodeling complexes play mechanistically distinct roles in ploidy maintenance.

We next assessed the ability of defective SPBs to nucleate microtubules by introducing a plasmid expressing *GFP-TUB1* (Fig. S2 b). We found that dead SPBs were defective in microtubule nucleation, as expected (Chial et al., 1999; Araki et al., 2006; Kupke et al., 2011; Chen et al., 2014). Interestingly, large-budded cells that contain multiple SPBs (ranging from three to nine SPBs per cell) had more than two SPBs that were able to nucleate microtubules and associate with DNA, suggesting that the supernumerary SPBs were at least partially functional. To test whether SPBs accumulate as ploidy increases, we quantified large-budded cells with SPB defects in haploid, diploid, and tetraploid *rsc2Δ* strains and found that tetraploid cells had an elevated number

of large-budded cells with multiple SPBs (Fig. S2 c). Thus, SPBs seem to accumulate as ploidy increases, suggesting that supernumerary SPBs might fail to segregate accurately in some instances.

To monitor SPB kinetics in cells transitioning from the haploid to diploid state, we created a glucose-repressible allele of *HTL1*, the *RSC* gene that caused the fastest diploidization rate when deleted (Fig. 1 b). The efficiency of the shut-off allele was assessed by monitoring the ploidy of wild-type and *htl1Δ* strains containing the glucose-repressible *HTL1* gene after growth in medium containing galactose (*HTL1* on) or glucose (*HTL1* off) (Fig. 3 b). The wild-type strain remained haploid regardless of the carbon source, whereas the *htl1Δ* strain was haploid when grown on galactose but fully diploidized after 20 generations of growth in medium containing glucose. Additionally, microscopic analysis showed that diploidization correlated with an increase in SPB defects (Fig. 3 c). Thus, the *HTL1* shut-off strain can be used for conditional induction of SPB defects and spontaneous diploidization.

A microfluidics system was used to monitor the effects of Htl1 depletion on SPB duplication in live cells over the course of 8 h
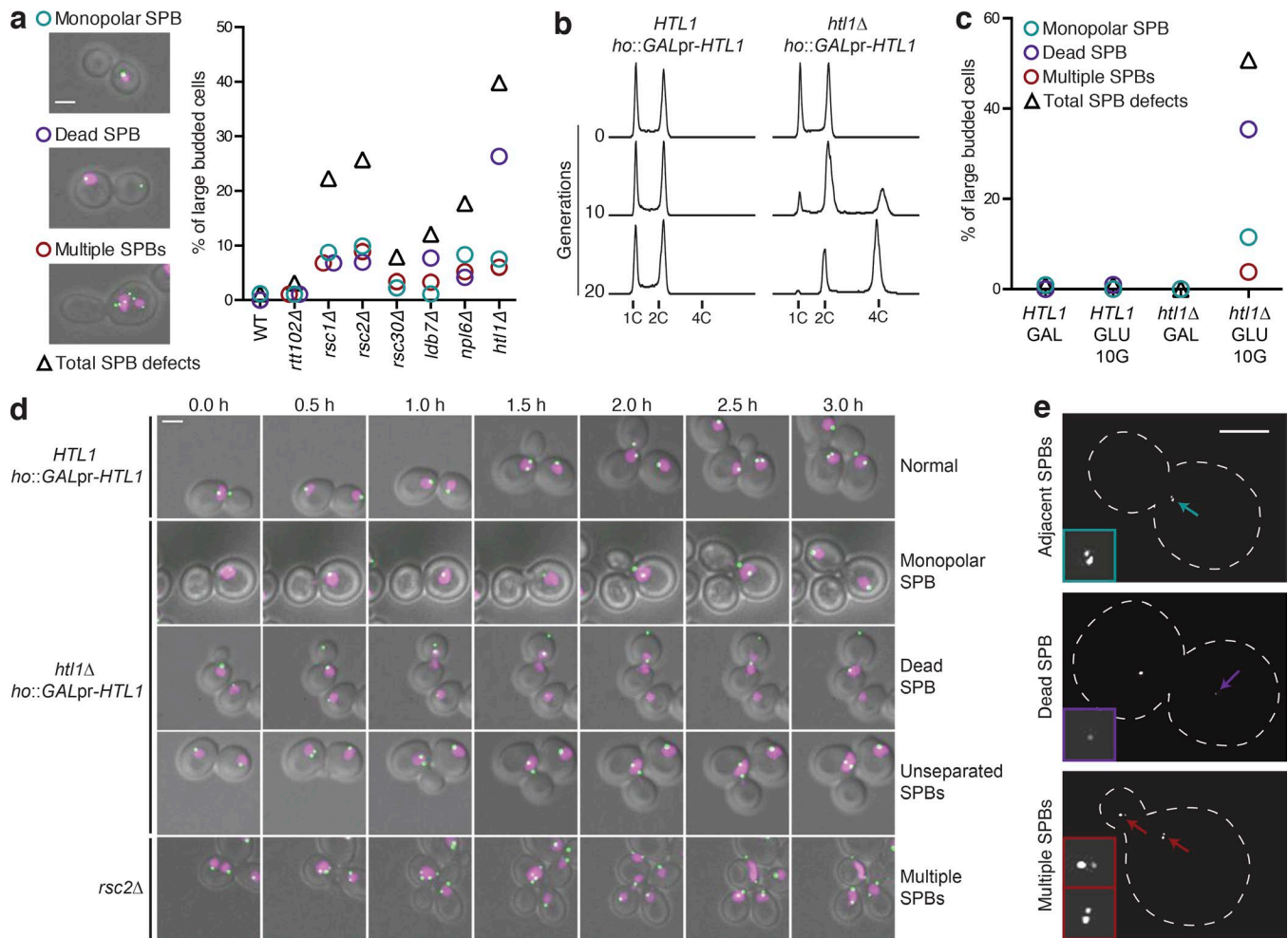
Figure 3. **The loss of nonessential RSC subunits causes defective SPB function. (a)** Haploid *rscΔ* spores expressing Spc42-GFP and Hta2-mCherry were freshly germinated and grown to logarithmic phase, and at least 100 large-budded cells were scored for the defects indicated in the micrographs (left). The mean of two technical replicates is plotted. The micrographs are maximum-intensity projections of representative cells containing the indicated SPB defect. Bar, 3 μm. **(b)** A glucose-repressible *HTL1* allele was integrated at the *HO* locus in a wild-type or *htl1Δ* strain. Expression of *HTL1* was repressed by the addition of glucose, and ploidy was analyzed by flow cytometry at the indicated times. **(c)** Samples from panel b were imaged, and SPB defects in large-budded cells were quantified as in panel a. At least 100 large-budded cells were scored for SPB defects. 10G, 10 generations. **(d)** Strains were grown in medium containing glucose for 12 h and then imaged in a microfluidic chamber, for the times specified, in rich medium containing glucose. Corresponding image sequences can be found in Videos 1, 2, 3, 4, and 5. Bar, 3 μm. **(e)** Maximum-intensity projections of representative *HTL1* shut-off cells containing Spc42-GFP after growth in glucose for 12 h, imaged using SIM. Each type of SPB defect is indicated and highlighted by a colored arrow. The insets show higher-magnification images of the SPBs that are highlighted by arrows. Bar, 3 μm. The corresponding flow cytometric analysis is shown in Fig. S2 d.

(Fig. 3 d and Videos 1, 2, 3, 4, and 5). Large-budded cells containing each of the indicated SPB defects were captured in real time. In the "monopolar SPB" series, only a single SPB is detected, and the DNA mass remains in the mother cell through 1.5 h. The mother then rebuds and undergoes a round of SPB duplication and segregation by 3 h. The result is three cells, one with no DNA and two that are presumably diploid. In the "dead SPB" series, the DNA mass remains associated with a single SPB, even though SPB duplication has occurred and the small daughter SPB has migrated into the bud by 0.5 h. By 3 h, the DNA mass has collapsed into the mother cell, which is presumably diploid, leaving a daughter cell with a SPB but no DNA. In the "unseparated SPB" series, the SPB in the cell on the left has duplicated by 0.5 h, but the SPBs do not become distantly separated and remain associated with a single, presumably diploid, DNA mass in the mother cell. The daughter

cell fails to receive any DNA or a SPB, although the mother cell now has two SPBs. We have observed that cells with two SPBs can enter the next cell cycle and rebud and duplicate both SPBs, resulting in the "multiple SPB" phenotype (shown for a *rsc2Δ* mutant, compare 0.5 h with 1 h). These data reveal that depletion of a single *RSC* gene can cause SPB duplication failure, dead SPBs, or multiple SPBs and that each of these SPB defects results in a nondisjunction event that causes diploidization. We also note that in all three SPB defects, a G_2/M delay was observed (Fig. S4 a), suggesting that the spindle assembly checkpoint is intact; however, after a few hours of arrest, cell cycle progression resumed.

The resolution of confocal microscopy is insufficient to distinguish adjacent but unseparated SPBs from SPBs that have failed to duplicate (Chen et al., 2014). To accurately define the defect in the monopolar SPB category, we used structured illumination

microscopy (SIM) to visualize large-budded cells containing Spc42-GFP before and after depleting Htl1 for 12 h (Figs. 3 e and S2 d). Large-budded cells with a truly monopolar SPB were not detected, indicating that Htl1 depletion does not cause defects in the first step of SPB duplication, when the satellite forms. Instead, we find that Htl1 depletion causes the accumulation of adjacent duplicated SPBs that have failed to separate. Additionally, we captured large-budded cells with very small dead poles, indicating that migration of a dead SPB into the bud requires only a small amount of Spc42-GFP. We also observed a budded cell that contained two pairs of adjacent SPBs (multiple SPBs) further supporting the idea that *rsc* mutant cells can duplicate supernumerary SPBs and suggesting that cells lack an SPB counting mechanism. Spc42-mCherry consistently colocalizes with another core SPB component, Spc29-GFP, indicating that we are detecting bona fide SPBs (Fig. S2 e).

RSC function in ploidy maintenance is independent of transcription

The canonical functions of RSC involve modulation of gene expression at the level of transcription (Angus-Hill et al., 2001; Damelin et al., 2002; Ng et al., 2002; Badis et al., 2008; Parnell et al., 2008), although transcription-independent RSC functions have been described: cohesin loading (Wong et al., 2002; Baetz et al., 2004; Huang et al., 2004; Liefshitz and Kupiec, 2011; Oum et al., 2011; Lopez-Serra et al., 2014), DNA damage repair (Sinha and Peterson, 2009), centromere remodeling required for kinetochore loading (Tsuchiya et al., 1998; Hsu et al., 2003; Desai et al., 2009; Verdaasdonk et al., 2012), and telomere maintenance (Ungar et al., 2009; Van de Vosse et al., 2013). Genome-scale studies to identify RSC transcriptional targets in the cell have been reported; however, the overlap between studies is small (Fig. S3 a; Angus-Hill et al., 2001; Damelin et al., 2002; Ng et al., 2002; Parnell et al., 2008). To identify RSC targets relevant to ploidy maintenance, we compared mRNA levels from haploid *rtt102Δ*, haploid *rsc1Δ*, haploid *rsc2Δ*, diploidized *npl6Δ*, and diploidized *htl1Δ* with a haploid wild-type strain and the mRNA levels in a wild-type or *htl1Δ* strain containing the glucose-repressible *HTL1* allele before and after growth in glucose for 24 h. We found only eight genes that were differentially regulated in at least three of five diploidizing strains (*rsc1Δ*, *rsc2Δ*, *npl6Δ*, *htl1Δ*, and the *HTL1* shut-off) but not in *rtt102Δ*. None had a known connection to SPB function or to DNA segregation, and overexpression of the three up-regulated genes (*HSP12*, *CPA2*, and *YGP1*) or deletion of the five down-regulated genes (*AGA1*, *BTN2*, *IMD2*, *MET6*, and *TIR1*) did not cause spontaneous diploidization (Table S2 and Fig. S3, b and c). Thus, it is unlikely that RSC regulates ploidy through a transcriptional mechanism.

The RSC complex promotes SPB insertion

To gain mechanistic insight into how RSC facilitates SPB duplication, we used synthetic genetic array (SGA) analysis to identify all genetic interactions for *rscΔ* alleles (Table S3). Because most *rscΔ* mutants diploidize rapidly, these genes are poorly represented in previous large-scale genetic interaction screens (Costanzo et al., 2010). However, we determined that SGA could be performed on fresh haploid isolates of *rsc1Δ*, *rsc2Δ*, *rsc30Δ*, and *ldb7Δ*. No gene

ontology enrichment was detected in the identified interacting genes; however, there was a large number of positive genetic interactions between RSC and SPB components (Fig. 4 a). To complement this finding, a high-copy-number plasmid containing each SPB component controlled by its native promoter (Magtanong et al., 2011) was transformed into the *HTL1* shut-off strain, and serial dilutions of cells were spotted onto medium containing galactose or glucose. Upon depletion of Htl1, a negative synthetic dosage interaction was observed with *MPS3* and *NDC1* (Fig. 4 b), both of which are important for insertion of new SPBs into the nuclear envelope during the SPB duplication cycle (Chial et al., 1999; Friederichs et al., 2011; Chen et al., 2014). Interestingly, this negative interaction corresponded to faster diploidization (Fig. 4 c). We also observed that overexpression of another SPB insertion factor, Nbp1, resulted in faster growth when Htl1 was depleted (Fig. 4 b). Surprisingly, overexpression of Nbp1, and no other SPB component, rescued the diploidization phenotype (Fig. 4 c), indicating that Nbp1 is limiting when Htl1 is depleted.

We reasoned that if insufficient Nbp1 is the cause of diploidization and SPB defects in *rsc* mutants, then the *rsc* mutants should display SPB insertion defects. The colocalization of the nuclear SPB component Spc110 with the core SPB component Spc42 is indicative of SPB insertion into the nuclear envelope (Friederichs et al., 2011). As Htl1 is depleted, large-budded cells with a single-focus–containing Spc42-mCherry and Spc110-GFP began to accumulate (Fig. 5, a and b, 2–4 h), indicating a delay in SPB separation. After 5–8 h of Htl1 depletion, large-budded cells with an uninserted SPB (a Spc42 focus with no associated Spc110; Fig. 5 b) accumulated, indicating a dramatic SPB insertion defect. The uninserted SPB was found almost exclusively in the bud (Fig. S4 b), in agreement with the location of the dead SPBs observed in our other experiments. Consistent with a model in which limiting Nbp1 is the cause of the observed insertion defect and resulting diploidization, increasing *NBP1* gene dosage partially ameliorated the SPB insertion defect caused by Htl1 depletion (Fig. 5 c). Together this suggests that overexpression of Nbp1 can delay spontaneous diploidization, but RSC likely plays an additional role in Nbp1 function at the SPB.

To obtain a high-resolution view of the SPB defects, we imaged cells during Htl1 depletion by transmission electron microscopy (TEM). The dead SPB appeared to be partially inserted into the nuclear envelope but failed to nucleate nuclear microtubules, resulting in the pulling of a tubule of nuclear envelope into the bud (Fig. 5 d, top and middle). The old SPB was found in an abnormal position at the bud neck, with nuclear microtubules evident (Fig. 5 d, bottom). We conclude that the dead SPB could be partially inserted into the nuclear membrane but is unable to bind Spc110 and thus unable to nucleate nuclear microtubules. This results in a failure to segregate any DNA from the mother cell, which would therefore become diploid.

Depletion of Htl1 causes altered NPC morphology and nuclear envelope abnormalities

We considered two models to explain how RSC promotes SPB insertion, one involving direct action of RSC at the SPB and the other involving RSC enhancing nuclear transport via the NPC. Although a large-scale study identified weak interactions
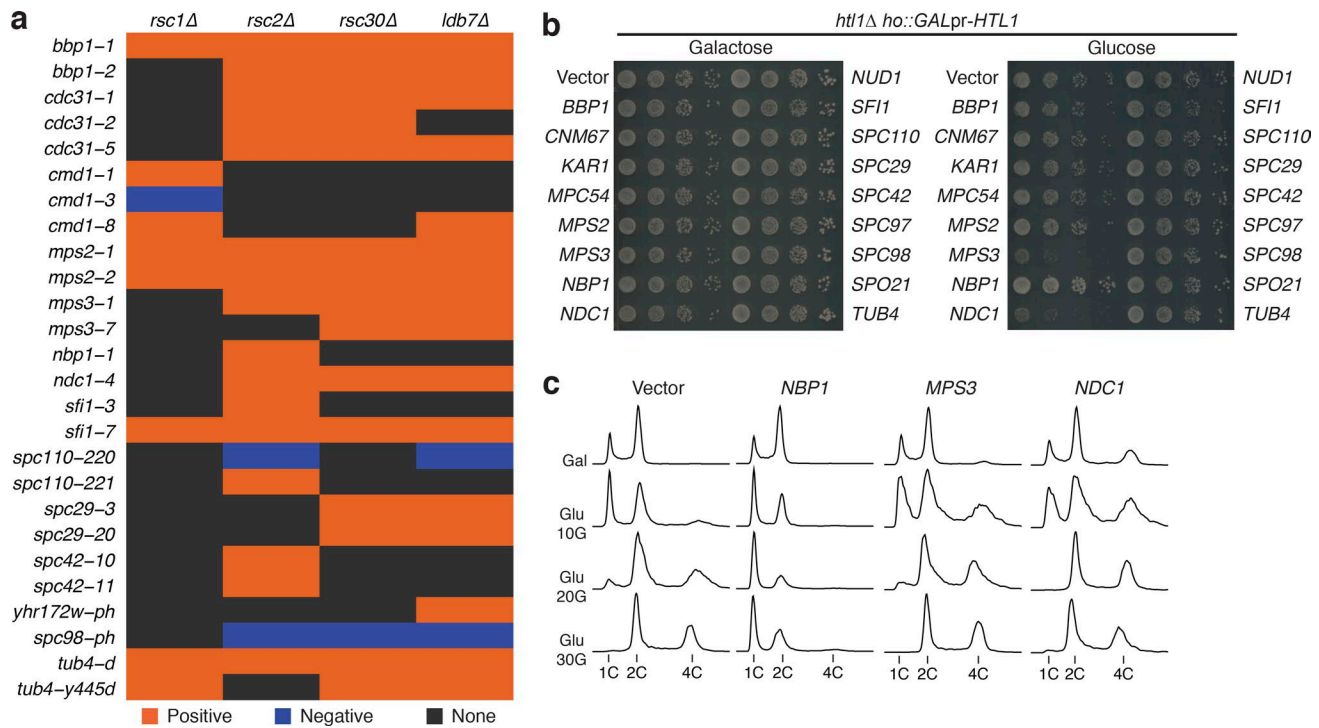
Figure 4. **RSC mutants show genetic interactions with SPB genes. (a)** The indicated *rscΔ* strains were subjected to SGA analysis. The SGA scores for *rscΔ* and temperature-sensitive SPB alleles are displayed as a heat map. Positive genetic interactions have SGA scores >0.080, and negative genetic interactions have SGA scores less than –0.080. **(b)** The *HTL1* shut-off strain was transformed with a high-copy-number plasmid expressing the indicated SPB component gene from its native promoter. Serial dilutions of each strain were spotted on medium containing galactose or glucose and grown for 3–5 d. **(c)** The indicated *HTL1* shut-off strains from panel b were grown in liquid medium containing galactose or glucose for the specified amount of time, and ploidy was monitored by flow cytometry.

between RSC and the SPB (Lambert et al., 2010) and the BAF180 subunit of the human RSC orthologue (PBAF) can be detected at spindle poles (Xue et al., 2000), we were unable to detect RSC-SPB interactions by yeast two-hybrid (Y2H; Fields and Song, 1989) or RSC at the SPB by bimolecular fluorescence complementation (BiFC; Sung and Huh, 2007; Fig. S3, d–f).

The RSC complex physically interacts with the NPC (Van de Vosse et al., 2013), is important for NPC assembly, and plays a role in maintaining nuclear envelope integrity (Titus et al., 2010). Furthermore, an *npl6* temperature-sensitive mutant is defective in nuclear transport of several proteins (Bossie and Silver, 1992), and a *rsc9-1* strain is defective in nuclear export of Kap121 (Damelin et al., 2002), all implicating RSC in NPC function. Because nuclear import of Nbp1 is critical for SPB insertion (Kupke et al., 2011), we examined the morphology of NPCs during Htl1 depletion (Figs. 6 a and S5 a). The NPC distribution changes from the typical uniform distribution at the nuclear periphery (time = 0) to an abnormal and punctate distribution at later times. The abnormal NPC distribution is an indicator of NPC and/or nuclear envelope stress (Titus et al., 2010; Meseroll and Cohen-Fix, 2016). We tested whether overexpression of *NBP1* rescued the NPC localization by quantifying pixel intensity in at least 100 cells containing Nic96-GFP or Nup170-GFP before and after Htl1 depletion. We found that depletion of Htl1 resulted in higher levels of Nic96-GFP aggregation compared with Nup170-GFP, suggesting that Htl1 has varying influences on specific Nup localization. Interestingly, overexpression of *NBP1* rescued Nic96-GFP morphology, suggesting that NPC

localization is influenced by SPB insertion defects rather than RSC depletion (Figs. 6 b and S5, b and c).

We examined individual NPCs using TEM and did not detect structural abnormalities; however, we did observe enrichment of NPCs on nuclear tubules that result from uninserted SPBs (Fig. 6 c). Interestingly, we also observed unusual nuclear envelope flares after Htl1 depletion in cells with SPB insertion defects (Fig. 6 d, left). The flares formed opposite to the old SPB (Fig. 6 d, right) and are consistent with excessive synthesis of the nuclear envelope, a feature that has been attributed to prolonged arrest at the spindle assembly checkpoint (Witkin et al., 2012). We propose that abnormal Nbp1 function results in SPB insertion defects that in turn lead to abnormal NPC morphology and nuclear envelope stress.

Htl1 influences the distribution of Nbp1 and Ndc1 to SPBs

To test whether RSC-dependent nuclear transport of Nbp1 through the NPC is responsible for ploidy maintenance, we used a plasmid to overexpress Nbp1-GFP from a strong *ADH1* promoter and examined Nbp1-GFP import after Htl1 depletion. Cells that lack the Nbp1 import karyopherin Kap123 accumulate Nbp1-GFP in the cytoplasm, as reported (Fig. 7 a; Kupke et al., 2011). In contrast, when Htl1 is depleted, Nbp1-GFP accumulates inside the nucleus in apparent aggregates that rarely colocalize with the SPB. We infer that RSC is not affecting transport of Nbp1 into the nucleus and that RSC function is important for proper association of Nbp1 with the SPB.
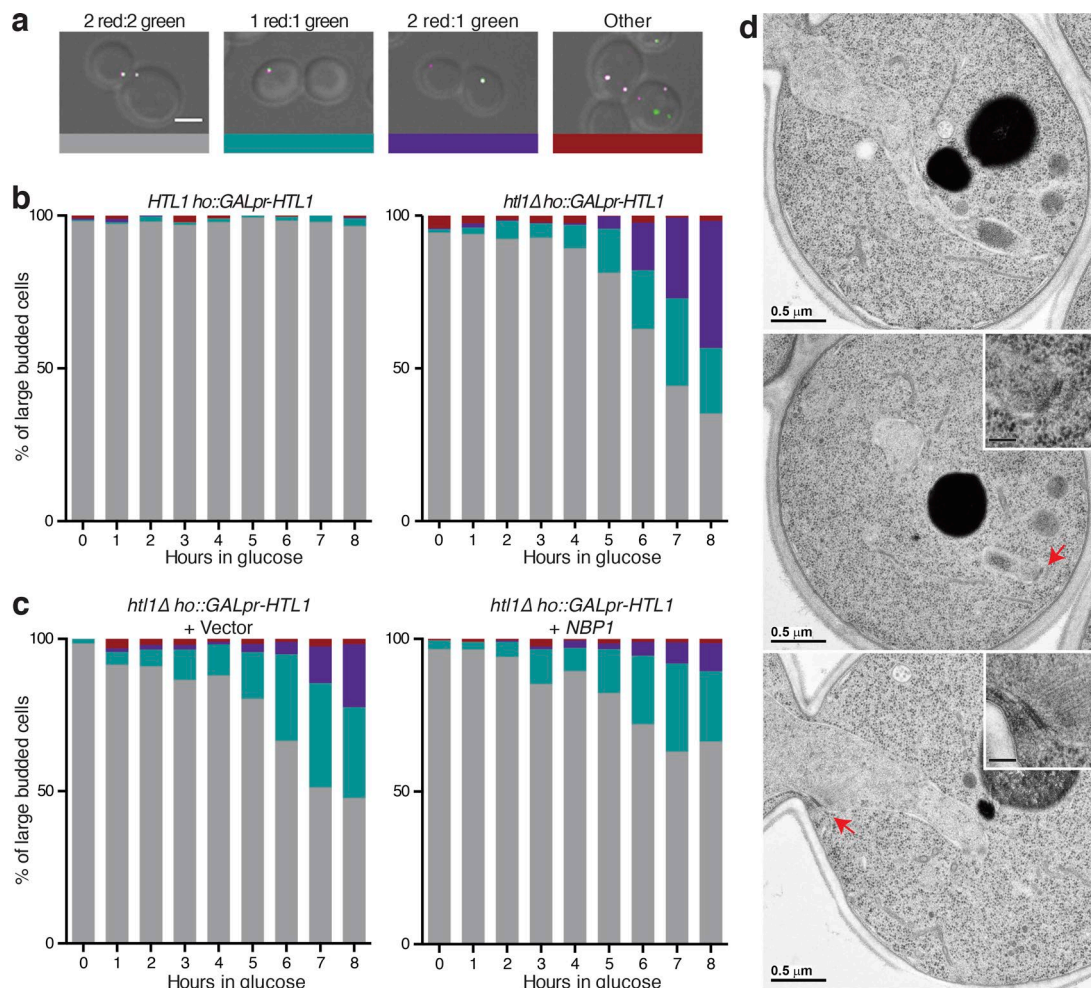
Figure 5. **Htl1 is important for SPB insertion into the nuclear envelope. (a)** SPB phenotypes in large-budded wild-type and *HTL1* shut-off cells expressing Spc110-GFP and Spc42-mCherry are shown. Images are maximum-intensity projections. Bar, 3 μm. **(b)** Wild-type and *HTL1* shut-off strains were grown in rich medium containing glucose for 8 h. Cells were imaged each hour, and at least 100 large-budded cells were assessed for the phenotypes depicted in panel a. **(c)** The experiment outlined in panel b was repeated with *HTL1* shut-off strains expressing Spc42-mCherry and Spc110-GFP and carrying either the empty vector or a high-copy plasmid expressing *NBP1* from its native promoter. **(d)** TEM was performed on an *HTL1* shut-off strain after 12 h of logarithmic growth in rich media containing glucose. All images are sections from the same large-budded cell. An abnormal nuclear protrusion (top), a dead SPB (red arrow; middle) and a mature SPB (red arrow; bottom) are shown. Bars: (large images) 0.5 μm; (insets) 0.1 μm.

To quantify the amount of Nbp1-GFP at the SPB (marked by Spc42-mCherry), we tagged chromosomal *NBP1* with GFP to reduce Nbp1-GFP variability caused by differences in plasmid copy number. We found that Nbp1-GFP caused rapid diploidization, so we also expressed a high-copy-number plasmid containing untagged *NBP1* controlled by its native promoter (Magtanong et al., 2011) to suppress ploidy changes. Nbp1-GFP was lost at dead poles after 8–12 h of Htl1 depletion, and Nbp1-GFP appeared to be absent from both SPBs after 24 h (Fig. 7 b). Quantification of Nbp1-GFP at >200 SPBs revealed a clear decrease in SPB-associated Nbp1 during Htl1 depletion (Figs. 7 d and S6, a–c) indicating that RSC is required for proper Nbp1 localization to the SPB. We next quantified the total cellular abundance of Nbp1 (Fig. 7 c). Little change in total Nbp1 abundance was evident when Htl1 was depleted, indicating that a decrease in total Nbp1 is unlikely to account for the loss of SPB-associated Nbp1 or for the loss of Nbp1 function that we observed.

Nbp1 binds directly to Ndc1, a SPB insertion factor that is also a component of the NPC (Araki et al., 2006). Thus, we measured the level of Ndc1 at SPBs and at NPCs (Figs. 7 e and S6, d–f). During Htl1 depletion, we detected a redistribution of Ndc1 from the SPB to the NPC, consistent with a failure to stabilize Ndc1 at the SPB because of the decrease in Nbp1 at the SPB. Given that depleting Htl1 does not affect Nbp1 transport into the nucleus or total Nbp1 levels, we conclude that RSC function is essential for normal Nbp1 localization to the SPB to promote redistribution of Ndc1 from the NPC to the SPB to catalyze insertion of the new SPB.

Discussion

We have defined the role of the RSC complex in ploidy maintenance. At least 15 of 17 RSC subunits have now been implicated in this role (this study and Lanzuolo et al., 2001; Yu et al., 2006; Campsteijn et al., 2007; Wang and Cheng, 2012; Imamura et al.,
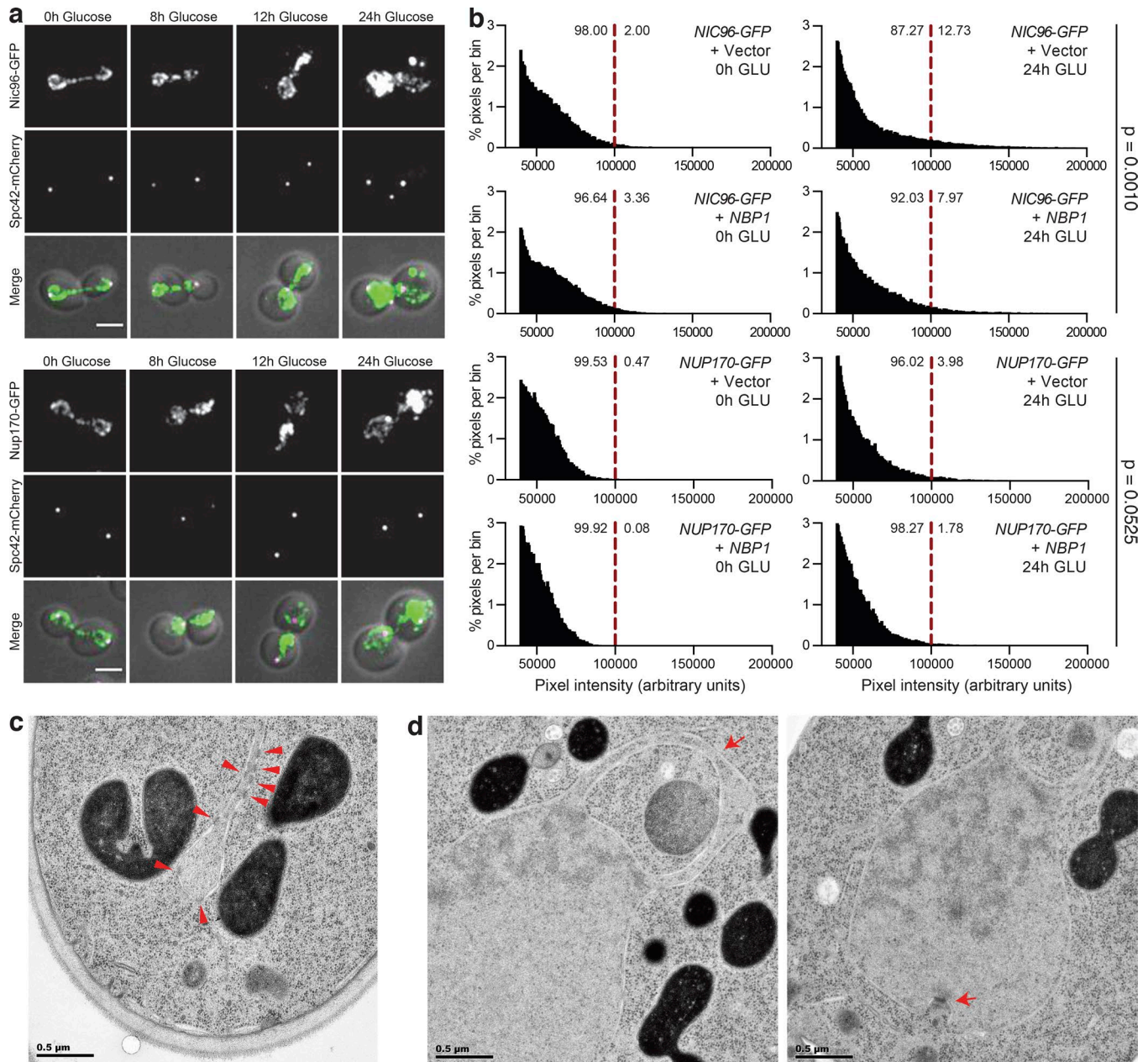
Figure 6. Htl1 depletion causes abnormal NPC morphology and nuclear envelope stress. (a) *HTL1* shut-off strains expressing the indicated GFP-tagged NPC proteins were grown in the presence of glucose and imaged at the indicated times. Maximum-intensity projections of representative large-budded cells are shown. Bar, 3 μm. Corresponding flow cytometry histograms can be found in Fig. S5 a. **(b)** Nic96- and Nup170-GFP intensity per pixel was measured as a proxy for NPC morphology. At least 100 *HTL1* shut-off cells were measured for each strain. Glucose shut-offs were performed in the absence (vector) and presence of *NBP1* overexpression. The distribution of GFP intensity per pixel is displayed, as is the percentage of pixels above and below 100,000 arbitrary units. The P values from a one-tailed Mann-Whitney test are shown. Corresponding flow cytometry histograms can be found in Fig. S5 b. **(c)** NPC structure (red triangles) was examined using TEM on an *HTL1* shut-off strain after 12 h of logarithmic growth in media containing glucose. A representative section showing eight NPCs on a nuclear tubule is shown. **(d)** TEM was performed on an *HTL1* shut-off strain after 12 h of logarithmic growth in media containing glucose. Both images represent sections from the same large-budded cell. An abnormal nuclear flare (red arrow; left) and a monopolar SPB (red arrow; right) can be seen. Bar, 0.5 μm.

2015), suggesting that the entire complex is important for preventing changes in the number of chromosome sets. Function in ploidy maintenance is an unanticipated role for RSC, independent of its characterized roles in regulating gene expression and other chromatin-related activities. By surveying the complete set of nonessential RSC subunits, we find that the contribution of each subunit to ploidy maintenance is not equivalent but that all *rsc* mutants, except *rtt102Δ*, find equilibrium at the diploid state, which results in distinct changes in cellular morphology. We identify the mechanism of ploidy gain in *rsc* mutants: complete genome missegregation caused by defective SPB morphogenesis. We define the SPB defect as a failure of the nascent SPB to insert properly into the nuclear envelope and to subsequently nucleate nuclear microtubules and capture the kinetochores.
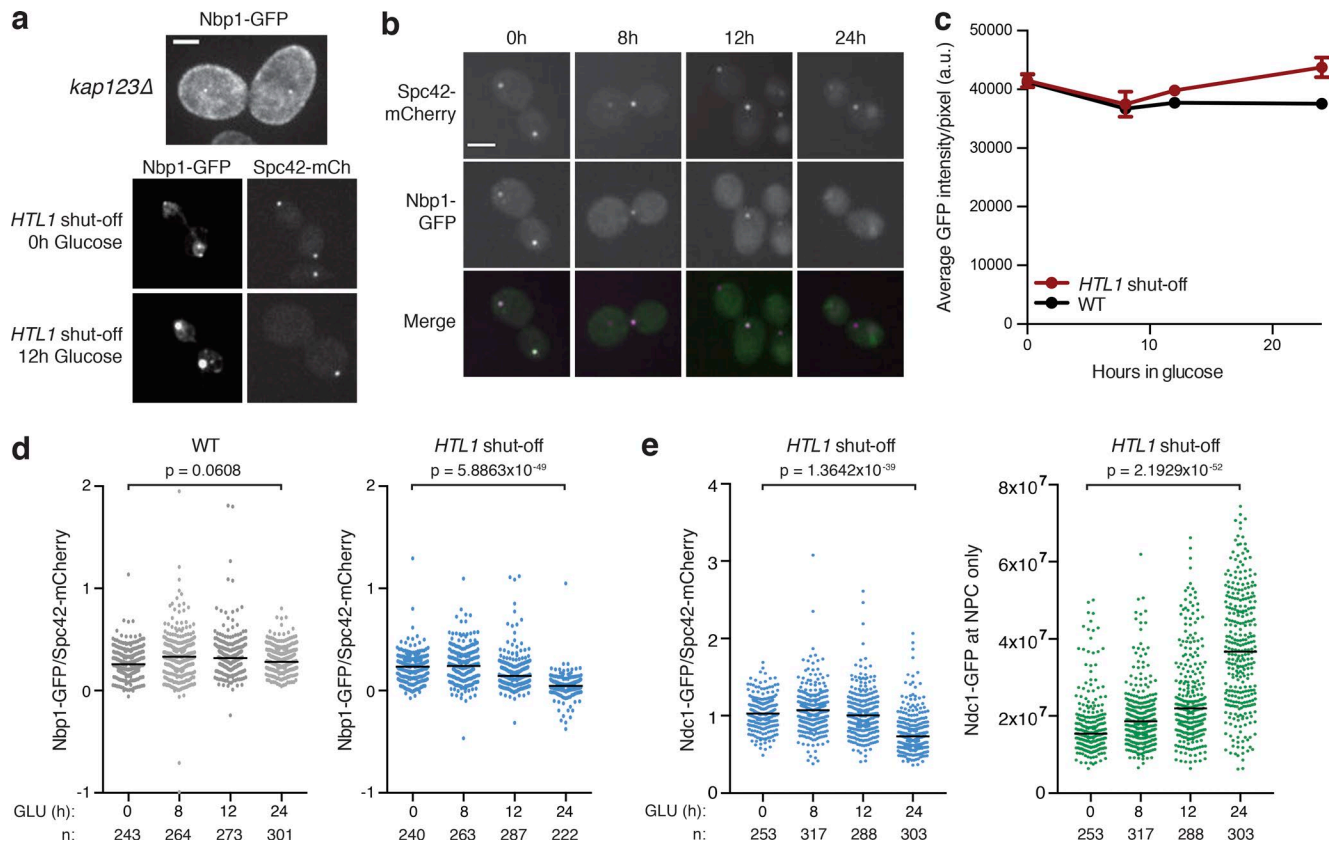
Figure 7. **Depletion of Htl1 causes decreased Nbp1 and Ndc1 at SPBs. (a)** Nbp1-GFP was expressed from the *ADH1* promoter in a *kap123Δ* strain or the *HTL1* shut-off strain containing Spc42-mCherry, and summed projections of a representative large-budded cell are shown. Bar, 3 μm. **(b)** Wild-type and *HTL1* shut-off strains expressing Nbp1-GFP and carrying a high-copy plasmid expressing *NBP1* were grown in medium containing glucose for the indicated times. A summed projection of a representative large-budded cell for each time point in the *HTL1* shut-off is shown. Bar, 3 μm. Corresponding flow cytometry histograms can be found in Fig. S6 a. **(c)** The mean GFP intensity per pixel in the whole cell was measured for 100 cells at the indicated times by using summed intensity projections from panel b. Error bars represent one SD from the mean. **(d)** Levels of Nbp1-GFP at >200 SPBs were measured in wild-type and *HTL1* shut-off strains carrying a high-copy plasmid expressing *NBP1* at the indicated times during growth in glucose. The ratio of Nbp1-GFP to Spc42-mCherry at the SPBs is plotted. The black bars represent the medians. **(e)** Levels of Ndc1-GFP at SPBs or NPCs were measured in the *HTL1* shut-off strain at the indicated times. The ratio of SPB-associated Ndc1-GFP to Spc42-mCherry for at least 200 SPBs is shown on the left. The amount of Ndc1-GFP at the NPC cells is displayed on the right. The black bars represent the medians. Corresponding flow cytometry histograms can be found in Fig. S6 d. The P values were calculated using a two-tailed Mann-Whitney test.

Further, we find that SPB insertion failure is the result of insufficient quantities of the insertion factors Nbp1 and Ndc1 at the SPB. Although many studies have observed a link between RSC and NPC function (Bossie and Silver, 1992; Damelin et al., 2002; Titus et al., 2010; Van de Vosse et al., 2013), we do not see defects in nuclear import of Nbp1. Because overexpression of Ndc1 does not rescue spontaneous diploidization in *rsc* mutants, our findings support a model where, after nuclear import of Nbp1, RSC is critical for effective localization of Nbp1 to the duplicating SPB, which allows Nbp1 to stabilize Ndc1 at the new SPB to promote SPB insertion and ploidy maintenance (Fig. 8).

SPB insertion influences inheritance

The recent discovery of the SPB inheritance network has defined the pathway that allows cells to differentiate the old and new SPB (Lengefeld et al., 2017). In wild-type cells, the preexisting SPB is marked by Swe1-dependent phosphorylation of Nud1 in G1 resulting in movement of the old SPB into the bud while the new SPB remains in the mother cell. In *rscΔ* cells, we find that the new, uninserted SPB migrates into the bud while the old SPB oscillates

between the mother and bud before residing in the mother with the duplicated genome (Video 3), indicating that proper SPB insertion of the new SPB into the nuclear envelope is required for normal SPB inheritance. We propose that the *HTL1* shut-off allele will be a valuable tool to understand the influence of SPB insertion on inheritance.

Absence of an SPB counting mechanism

Mutants in *rsc* delay in G2/M, yet ultimately proceed through mitosis and cytokinesis, resulting in the production of anucleate cells coincident with increased ploidy of the mother cell. Thus, the *rsc* mutants activate and adapt to the spindle assembly checkpoint. The process of passing through mitosis and cytokinesis without chromosome segregation can lead to both SPBs remaining in the mother cell (see example in Fig. 3 d) and then duplication of both SPBs at G1/S of the next cell cycle (Video 5). We conclude that the relicensing of SPBs for duplication, presumably by dephosphorylation of the half-bridge component Sfi1 (Avena et al., 2014; Elserafy et al., 2014), occurs normally in *rsc* mutants despite the presence of supernumerary SPBs.
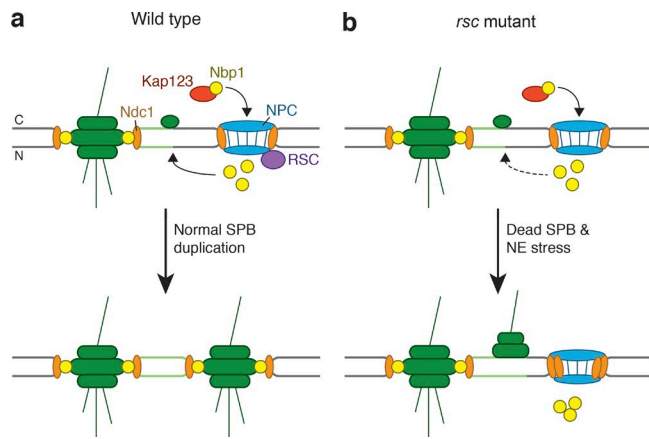
Figure 8. **Model of RSC-dependent distribution of Nbp1 and Ndc1 to the new SPB.** Kap123 targets Nbp1 to the NPC for import from the cytoplasm (C) into the nucleus (N). **(a)** In wild-type cells, RSC facilitates appropriate distribution of Nbp1 to the duplicating SPB. Nbp1 stabilizes Ndc1 at the new SPB, which promotes SPB maturation. The new SPB is then able to nucleate both cytoplasmic and nuclear microtubules to facilitate accurate chromosome segregation and ploidy maintenance. **(b)** In *rscΔ* mutants, Nbp1 distribution is compromised, resulting in the loss of Ndc1 at SPBs and an accumulation of Ndc1 at NPCs, resulting in nuclear envelope (NE) stress. The resulting dead SPB is able to nucleate microtubules from the cytoplasmic side but not from the nuclear side, resulting in a nondisjunction event and spontaneous diploidization.

Furthermore, as many as 9% of large-budded cells have multiple SPBs in *rscΔ* populations (Fig. 3 a, *rsc2Δ*; and Video 5), ranging from three to as many as nine SPBs in a single cell, and accumulation of supernumerary SPBs correlates with ploidy increase, indicating that SPB duplication cycles continue in the presence of abnormal SPB numbers. Finally, we find that the supernumerary SPBs are able to nucleate microtubules (Fig. S2 b) and contain at least two core SPB proteins (Fig. S2 e), suggesting that multiple SPBs are the product of the normal SPB duplication process and not the result of SPB fragmentation. Thus, although SPB duplication is limited to once per cell cycle by licensing Sfi1 (Avena et al., 2014; Elserafy et al., 2014), yeast cells do not seem to have the ability to detect extra SPBs. It will be of interest to determine whether the absence of SPB counting is unique to *rsc* mutants or is a property of wild-type cells.

RSC influences Nbp1 and Ndc1 distribution
The distribution of Ndc1 between the SPB and NPC is dependent on another SPB factor, Mps3 (Chen et al., 2014). In our setting, we find that Nbp1 is the key ploidy maintenance factor that becomes limiting when RSC is depleted and that Nbp1 does not accumulate appropriately at the SPBs in the absence of RSC. This results in alteration of Ndc1 distribution where we observe loss of Ndc1 at the SPB and gain at the NPC. Superresolution microscopy shows that Nbp1 is the last SPB component to localize to the duplicating SPB (Burns et al., 2015), and our data suggest localization of Nbp1 is critical for maintaining Ndc1 at SPBs to facilitate SPB insertion. Additionally, we observe NPC aggregation and abnormal nuclear envelope flaring when Htl1 is depleted, which corresponds with an increase of Ndc1 at NPCs. Thus, increased Ndc1 at the NPCs could contribute to abnormal NPC morphology and

nuclear envelope flaring. A key question that remains is how RSC specifically influences Nbp1 localization to the SPB. RSC does not regulate Nbp1 levels or facilitate Nbp1 nuclear transport, and so RSC must promote Nbp1 localization to the SPB through an alternative mechanism, which remains to be discerned.

The drive to diploidy
Previous studies with wild-type *S. cerevisiae* strains have revealed a drive for particular ploidy states under specific stress conditions (Gerstein et al., 2006). We find that *rscΔ* mutants, like wild-type yeast, exist predominantly in the diploid state. We propose that *rscΔ* mutants have difficulty reaching a critical threshold of Nbp1, resulting in delayed SPB duplication and insertion and spontaneous diploidization. The modest increase in fitness observed in our growth analyses suggests that diploidized cells are better able to tolerate the SPB defects observed in *rscΔ* cells. Perhaps this is because of gene dosage differences acquired from autodiploidization or perhaps the increased cell size and accompanying increase in protein biosynthesis (Marguerat and Bähler, 2012). Such tolerance does not scale with ploidy, because we see no evidence of tetraploidization of *rsc* mutants, even though wild-type tetraploids are stable. The aneuploidy and reductional division that we see when we force *rsc* mutants to tetraploidize is reminiscent of the gain-in-ploidy/aneuploidy vector followed by some tumor cells (Davoli and de Lange, 2011) and so could be a useful model for that mode of oncogenesis.

RSC homologues in metazoans
We have established a role for RSC in Ndc1 and Nbp1 distribution to the duplicating SPB, a critical step for SPB insertion and subsequent ploidy maintenance in budding yeast. Interestingly, the mammalian RSC homologue PBAF (SWI/SNF-B) localizes to centrosomes (Xue et al., 2000), and mutations in the PBAF subunit *hSNF5* (the homologue of yeast *SFH1*) are present in aggressive polyploidized cancer cells (Isakoff et al., 2005; Vries et al., 2005). Despite the differences in centrosome biology between yeast and humans, our study reveals that RSC can facilitate ploidy maintenance by mechanisms distinct from gene expression regulation and raises the possibility of a general role for RSC in regulating the function of microtubule-organizing centers. Moreover, because ploidy increases and chromosome segregation errors both contribute to genome instability and cancer progression (Davoli and de Lange, 2011), such a novel role for SWI/SNF-related complexes might be exploited therapeutically (St Pierre and Kadoch, 2017).

Materials and methods
Yeast strains and media
Yeast strains used in this study (Table S4) are derivatives of BY4741, BY4742, or BY4743 (Brachmann et al., 1998) with the exception of Y8800 and Y8930, which are derivatives of W303. Strains were constructed using standard yeast techniques, and, unless otherwise stated, standard yeast media and growth conditions were used (Sherman, 2002). Medium containing galactose contains 2% galactose and 1% raffinose instead of 2% glucose. Plasmids used in this study are listed in Table S5.

Heterozygous *rscΔ* strains were sporulated on solid sporulation medium for at least 1 wk at 23°C; tetrads were dissected and grown at 30°C for 2–4 d until colonies were large enough for replica plating for genotyping. Once appropriate strains were obtained, *rscΔ* mutants were used immediately for experimentation and were never stored at 4°C (low temperature causes rapid diploidization). For long-term storage, freshly germinated *rscΔ* strains were grown in liquid medium to saturation (10 generations) and stored at –80°C in 18% glycerol. When thawing *rscΔ* strains, the number of generations was closely monitored to ensure that the ploidy state was known.

Wild-type tetraploid strain CCT3 was a gift from M. Dunham (University of Washington, Seattle, WA). Tetraploid *rsc2Δ* and *htl1Δ* homozygotes were created by placing a single *MAT**a**/**a*** and *MATα/α* cell together on a YPD plate by using a dissection microscope. Plates were incubated for 3 d, and ploidy was checked by flow cytometry (described below; Bellay et al., 2011). The *HTL1* shut-off allele was made by amplifying the *GAL1,10* promoter, the *HTL1* gene, and the *URA3MX* cassette from pBY011-*HTL1* (Hu et al., 2007) followed by co-integration at the *HO* locus. GFP-tagged constructs were amplified from GFP collection strains (Huh et al., 2003). The Hta2-mCherry allele was amplified from MC193, and Spc42-mCherry was tagged using *pKT-mCherry-hphMX* (gifts from M. Cox in B. Andrews's laboratory, University of Toronto, Toronto, Canada).

For TSY152 and TSY153, the presence of p5587-*NBP1-kanMX* was required to keep the strain in the haploid state. We found that even in a wild-type strain (TSY152), GFP tagging the chromosomal *NBP1* allele caused spontaneous diploidization. For TSY169, an *HTL1* shut-off strain containing Spc42-mCherry was plated onto medium containing galactose and 5-FOA to select for cells that no longer expressed Ura3 from the *URA3MX* cassette marking the galactose-inducible *HTL1* allele at the *HO* locus. The resulting strain was grown on SD minus uracil plates to confirm the loss of a functional Ura3 gene and then transformed with pTK239 (gift from E. Schiebel, Universität Heidelberg, DKFZ-ZMBH Allianz, Heidelberg, Germany) and selected on SD minus uracil plates.

Diploidization assay
A colony originating from a freshly germinated spore was used to inoculate a 5-ml culture and incubated for 24 h at 30°C. If the culture was saturated (i.e., had an OD_{600} ≥10), a 100-μl sample was allowed to grow in fresh YPD for 4–6 h and then was fixed for flow cytometric analysis. Cells from the saturated culture were also used to inoculate a fresh 5-ml culture 1 in 1,000, and the cycle was repeated 10 times (i.e., for ~100 generations of growth). If a strain had an OD_{600} <10 after incubation for 24 h at 30°C, cells were allowed to incubate for additional 12-h increments until an OD_{600} ≥10 was reached.

Flow cytometry
Cells were prepared for flow cytometry as in Bellay et al. (2011). In brief, harvested cells were fixed in 70% ethanol for at least 15 min at room temperature, washed with water, and incubated in 0.2 mg/ml RNaseA (BioShop) in 50 mM Tris, pH 8.0, for 2 h at 37°C. Samples were then resuspended in 50 mM Tris, pH 7.5, containing

2 mg/ml proteinase K (BioShop), incubated at 50°C for 40 min, and resuspended in FACS buffer (200 mM Tris, pH 7.5, 200 mM NaCl, and 78 mM $MgCl_2$). Cells were stained with 2× SYBR Green (Life Technologies) in 50 mM Tris, pH 7.5. The samples were briefly sonicated and analyzed by using a Becton Dickinson FACSCalibur. Data were analyzed by using FlowJo Flow Cytometry Analysis Software and plotted on a linear scale unless otherwise stated.

Growth assays
Saturated cultures were diluted to OD_{600} = 0.0625 in 100 μl of YPD and transferred to a 96-well flat-bottom plate. The wells were sealed, and growth was monitored in a TECAN microplate analyzer by measuring OD_{600} every 10 min for 2,000 min. The plate was incubated at 30°C and agitated between measurements for the duration of the experiment. Wells containing only YPD medium were used to normalize the OD_{600} measurements, and the corrected values were plotted to make growth curves. The maximum slope (m_{max}) was determined by using a growth-rate algorithm in R designed by D. Carpenter in D. Botstein's laboratory (Princeton University, Princeton, NJ). The maximum doubling time was then calculated using the formula $\ln(2)/m_{max}$. The difference between haploid and diploid strains containing the same *rscΔ* was considered statistically supported if the P value was <0.05 by a one-tailed Student's *t* test.

Viability assay
Cells were grown overnight in rich medium to mid-logarithmic phase. A 500-μl sample was harvested at 5,000 rpm for 2 min. Cells were resuspended in 10 μl of filter-sterilized 0.01% methylene blue dye in 2% sodium citrate and incubated for 5 min at room temperature. 10 μl of sterile H_2O was added to the cells and incubated for 5 min. 3 μl of stained cells were spotted onto a microscope slide and covered with a glass coverslip. Cells were imaged on a Nikon Eclipse E400 light microscope. For each sample, 200 cells were scored by eye as white (alive) or blue (dead).

Detection of morphological mutants
We focused on two traits of cell morphology: cell size (C101_A1B) and roundness of bud (C114_A1B) at S/G_2 phase. Morphological abnormality of 4,718 mutants in the two traits were tested by a one-sample two-sided test with normal distribution after Box-Cox power transformation with 126 replicates of *his3Δ*, as described previously (Ohya et al., 2005). To estimate false discovery rate, P values of 4,718 mutants of the two traits were subjected to qvalue function in the qvalue package (Storey, 2002) of R (https://cran.r-project.org/). At a false discovery rate of 0.05, 532 and 392 of the 4,718 mutants had a statistically supported difference in the cell size (C101_A1B) or in roundness of bud (C114_A1B) at S/G2 phase, respectively.

PCA of morphological data
Morphological data for 109 replicates of diploid BY4743 cells (Ohya et al., 2015), 4,718 haploid deletion mutants of nonessential genes, and 126 replicates of the *his3Δ* control strain (Ohya et al., 2005) were used. For each morphological trait, the data for 4,718 mutants and 109 replicates of BY4743 were normalized by Box-Cox power transformation with 126 replicates of

the *his3Δ* control, as described previously (Ohya et al., 2005). We selected 254 of 501 traits to have normality in transformed data of *his3Δ* at P > 0.5 by the Shapiro-Wilk test as described previously (Ohya et al., 2005). Z values of *his3Δ* and BY4743 were subjected to PCA with the 254 traits, followed by projection of Z values of 4,718 mutants. PC1 and PC2 explained 87.1% and 3.2% of variance, respectively. Of the 254 traits, 120 traits had significant PC loadings for PC1 at >0.6 of absolute value of PC loading (P < 1.10^{-22} after Bonferroni correction, by Student's *t* test). The 120 traits were classified into 10 groups by a hierarchical cluster analysis with complete linkage of dissimilarity (1 − |correlation coefficient|) among 126 replicates of *his3Δ* and are listed in Table S1.

Normalization of newly acquired morphological data and projection onto PCs

New morphological datasets were acquired for 11 replicates of BY4741, 5 replicates of BY4743, 5 replicates of a *MAT**a***/*MAT**a*** diploid, and 3 replicates of each temperature-sensitive mutant of *STH1*, as described (Ohya et al., 2005). For each morphological trait, the data were normalized by Box-Cox power transformation with 126 replicates of haploid *his3Δ*. The mean of the Z value calculated from the 11 replicates of BY4741 in each trait was subtracted from Z values of the newly acquired morphological data. Subsequently, the Z values were projected onto the PC1 and the PC2 calculated by Z values of *his3Δ* and BY4743 with the 254 traits, as described above.

Fluorescence microscopy

For static imaging of live cells, 1 ml of logarithmically growing cells at OD_{600} = 0.5 (or equivalent) was harvested, washed in low-fluorescence medium twice, and resuspended in 5–10 µl of low-fluorescence medium. Then, 3 µl of cells was spotted onto a microscope slide and covered with a glass coverslip. For live-cell imaging, 300 µl of logarithmically growing cells in YPD was loaded into CellAsic ONIX haploid plates (Y04; Millipore), which were controlled with the Microfluidic Perfusion Platform (model Ev-262).

For (Fig. 5, a–c), strains were grown in YPGR overnight to mid-logarithmic phase. Cells were washed in YPD twice, resuspended in fresh YPD medium, and cultured for 8 h. Every hour, a 1-ml sample was removed, and the cell density was adjusted to keep cells in logarithmic phase. Each sample was fixed immediately by incubation in 4% PFA in 3.4% sucrose at room temperature for 15 min. The PFA was quenched with 200 mM glycine at room temperature for 10 min. The fixed cells were washed with 0.1 M KPO_4/sorbitol buffer twice and resuspended in 5–10 µl of 0.1 M KPO_4/sorbitol buffer. Samples were stored at 4°C until imaged on a confocal microscope. Fixed cells produced the strongest fluorescent signals if imaged within 48 h.

For all imaging except Fig. S2 e, confocal images were acquired with a Leica DMI6000 microscope equipped with an HCX PL APO 63× oil 1.40–0.60 NA objective by using Volocity imaging software (PerkinElmer) and a Hamamatsu ImageM EM-CCD digital camera. GFP was excited with a 491-nm laser line, and mCherry was excited with a 561-nm laser line. Images represent a projection of 11 z-slices taken with 0.4-µm step size

for each channel. For Fig. S2 e, selected confocal images were acquired with a Nikon Eclipse TI microscope equipped with an Apo TIRF 100× oil 1.49 NA objective and a Yokogawa CSU W1 spinning disk set to use the 50-µm pinhole wheel. The detector was an Andor DU897 EMCCD. All excitation was accomplished with a 405/488/561/640 dichroic, and GFP was excited with a 488-nm laser line, and mCherry was excited with a 561-nm laser line. GFP emission was collected through an ET525/36m filter, and mCherry emission was collected through an ET605/70m filter. Images represent a projection of 17 z-slices taken with 0.4-µm step size for each channel.

For SIM, cells were fixed in 4% PFA (Ted Pella) in 100 mM sucrose for 15 min at room temperature and then washed twice in phosphate-buffered saline, pH 7.4. SIM images were acquired with an Applied Precision OMX Blaze (GE Healthcare) as described (Burns et al., 2015).

All microscopy was performed at room temperature, and images were processed by using FIJI (ImageJ, National Institutes of Health).

SGA analysis

A diploid query strain was created by mating Y7091 with Y7092. The resulting diploid was transformed with PCR-amplified *natMX* cassette (from the plasmid p4339) containing homology to the 5′ and 3′ UTR of each *RSC* gene. Each resulting deletion was confirmed by PCR and then sporulated on solid sporulation medium for at least 1 wk at 23°C. Tetrads were dissected, and plates were incubated at 30°C for 2 d. Strains were genotyped by replica plating onto appropriate medium, and plates were incubated for an additional day at 30°C. The colony with the desired genotype was used to inoculate a YPD culture to make lawns for SGA. Standard SGA protocols were then followed (Tong et al., 2001). In brief, the freshly germinated *rscΔ* query strain was mated to the arrayed haploid yeast deletion collection or haploid yeast temperature-sensitive allele collection. Colonies were transferred to appropriate media to select for diploids, to sporulate diploids, and to select for *MATa* haploid cells containing both mutations. Each screen was performed once with each double mutant having four replicate colonies. Colony size was measured and compared with each single mutation as described previously (Costanzo et al., 2010). If the size of the double-mutant colony was greater than or less than expected, based on a multiplicative model of the single mutations alone, then genetic interactions were scored as positive or negative, respectively.

Dosage suppression spot assay

Plasmids from the MoBy-ORF v2.0 collection (Magtanong et al., 2011) containing the indicated SPB genes were transformed into the *HTL1* shut-off strain, and transformants were selected on synthetic medium containing galactose and lacking leucine (SGR-leu). Colonies were grown to saturation in liquid SGR-leu media. Cell density was measured, and each culture was diluted to an OD_{600} of 0.5 in a total volume of 200 µl in a 96-well flat bottom plate. 10-fold serial dilutions were made in adjacent wells, and cells were pinned onto SGR-leu plus G418 or SD-leu plus G418. Plates were incubated at 30°C for 3–5 d and imaged using a Canon CanoScan 8800F Scanner.

TEM

Cells were grown to logarithmic phase in YPGR, washed with YPD, and grown in YPD for 12 h. Cells were harvested and frozen on a high-pressure freezer (EM ICE; Leica) at ~2,050 bar, transferred under liquid nitrogen into 2% osmium tetroxide/0.2% uranyl acetate/acetone, and transferred to an automatic freeze substitution (AFS2) chamber (Leica) at –140°C. The freeze substitution protocol was as follows: –90° raised to –80° over 60 h, –80° raised to –60 over 5 h, held at –60 for 4 h, –60 to –20° over 5 h, held at –20° for 4 h, –20° to 0° over 4 h, and held at 0° for 5 h. Next, samples were removed from the AFS2, incubated at room temperature for 1 h, washed with acetone four times over 1 h, and removed from the planchettes. Samples were embedded in acetone/epon mixtures to final 100% epon as described previously (McDonnald, 1999). Finally, 50-nm serial thin sections were cut on an ultramicrotome (model UC6; Leica), stained with uranyl acetate and Sato's lead, and imaged on a transmission electron microscope (Tecnai Spirit; FEI).

Image quantification

Quantification of Nbp1-GFP at SPBs or Ndc1-GFP at the SPB and NPC was performed with custom plugins (available at http://research.stowers.org/imagejplugins) written for ImageJ as described (Chen et al., 2014). In brief, SPBs marked with Spc42-mCherry were used to determine the boundary of the SPB. This boundary was applied to the GFP channel to measure Nbp1- or Ndc1-GFP levels at the SPB. To measure Ndc1-GFP at the NPC, Ndc1-GFP at the nuclear periphery was measured, excluding the pool of Ndc1-GFP at the SPB. For Nbp1-GFP, the edge of the SPB was extended by 1 pixel to obtain a measurement of background cellular fluorescence. This value was then subtracted from the SPB value to obtain a more accurate measure of Nbp1-GFP at the SPB. A difference in Nbp1-GFP at SPBs or Ndc1-GFP at the SPB and nuclear envelope after growth in media containing glucose for 0 h or 24 h was considered statistically supported if the P value was <0.05 by a two-tailed Mann-Whitney test. Quantification of Nbp1-GFP in the whole cell was performed in ImageJ. The GFP background signal was identified by using an Otsu threshold (Otsu, 1979) on summed projections of confocal images, and these pixels were set to "not-a-number" and subtracted from the entire image. Then, the mean GFP intensity per pixel was measured for at least 100 cells.

Quantification of NPC aggregation was performed on summed projections of confocal images in ImageJ. First, the background signal was set to "not-a-number" and subtracted from images by using a default threshold of 40,000 arbitrary units. A bin size of 500 arbitrary units was applied, and the resulting values were plotted. The threshold for NPC aggregation was determined by manually measuring pixel intensity at abnormal NPCs and setting a value that was below all pixels found in altered NPCs (100,000 arbitrary units). A one-tailed Mann-Whitney test was used to test whether the distribution of Nup-GFP intensity decreased when *NBP1* was overexpressed compared with the empty vector control after Htl1 was depleted for 24 h. A P value <0.05 was considered to indicate statistical support.

CGH

After germination of heterozygous *rscΔ* strains, the ploidy of each strain was monitored by flow cytometry (Fig. 1 b). Genomic DNA from the sample that contained >95% diploid cells with the lowest number of generations was isolated. Genomic DNA from wild-type cells arrested in G_1 with α-factor was used as the control sample. CGH was performed essentially as described previously (Dion and Brown, 2009; Chambers et al., 2012). In brief, genomic DNA was amplified by using a WGA2 kit (Sigma) and treated with DNaseI (NEB) to fragment DNA to a mean 50-bp length. Then, DNA fragments were labeled with biotin-N^6-ddATP (Enzo Life Sciences) by using terminal deoxynucleotidyl transferase (Fermentas), hybridized to an *S. cerevisiae* Tiling Array (Affymetrix), and visualized using streptavidin R-phycoerythrin conjugate (Invitrogen) and normal goat IgG (Sigma). Experiment signal intensities from each microarray were compared with the control sample using Tiling Analysis Software (Affymetrix) using quantile normalization, perfect match probes only, a bandwidth of 60, maximum gap of 80, and minimum run of 40. The CGH profiles were generated with IGB 6.3 (Affymetrix).

Mating-type PCR assay

Genomic DNA was isolated from cells using the MasterPure Yeast DNA Purification kit (Epicentre). PCRs were performed by using an α-specific forward primer (5′-GCACGGAATATGGGACTACTT CG-3′) and a reverse primer that corresponded to sequence flanking either the 3′ UTR of the *MAT* locus (5′-AGTCACATCAAGATC GTTTATGG-3′), or the 3′ UTR of the *HMLα* locus (5′-TGTTACGGA GATGCAAAGCT-3′). Standard PCR methods were used with Taq polymerase (Invitrogen) with an annealing temperature of 49°C. Amplified DNA was separated on a 1% agarose gel alongside a 1-kb DNA ladder (FroggaBio) and imaged using a GelDoc XR (BioRad).

RNA sequencing and data analysis

Freshly germinated wild-type and *rscΔ* strains or a wild-type or *htl1Δ* strain containing a glucose-repressible *HTL1* allele was grown to logarithmic phase, and total RNA was isolated by using a RiboPure-Yeast kit (Ambion). Polyadenylated RNA species were captured by oligoDT beads (Illumina) and sequenced at the Donnelly Sequencing Facility by using the HiSeq 2500 (Illumina), multiplexing 18 samples per lane. The number of reads per sample ranged from 10.6 to 14.1 million. Data were analyzed using Galaxy (Afgan et al., 2016) by using the Tuxedo protocol (Trapnell et al., 2012). Reads were mapped to the SacCer3 reference genome downloaded from the *Saccharomyces* Genome Database website using TopHat. Mapped reads were assembled into transcripts using Cufflinks. Assembled transcripts and mapped reads were combined with Cuffmerge, and differentially expressed genes were identified with CuffDiff. Annotations in Table S2 were accessed from the *Saccharomyces* Genome Database using g:Convert from g:Profiler (Reimand et al., 2016). Raw sequencing data can be accessed on GEO Omnibus with accession no. GSE106768.

BiFC

*MAT**a*** strains expressing VN-fusion proteins and *MATα* cells expressing VC-fusion proteins were mated on YPD plates and grown overnight at 30°C, and diploids were selected by growth on SD –ura +G418 plates. The resulting diploids were grown to mid-logarithmic phase in YPD, and live cells were imaged by

using Volocity imaging software (PerkinElmer) controlling a Leica DMI6000 confocal fluorescence microscope.

Y2H

NUD1, *BBP1*, *RSC30*, *RTT102*, and *SPC110*, were amplified from BY4741 with primers containing attB sites. *Escherichia coli* strains carrying the BG1805 plasmids containing all other ORFs of interest flanked by attB sites were purchased from GE Healthcare Life Sciences. Each ORF was transferred to the donor plasmid pDONR-201or pDONR-221, which was used as the entry vector for the Gateway protocol (Invitrogen). In brief, the entry vector containing the ORF of interest was recombined with destination plasmids containing either the Gal4 activation domain (pDEST-AD) or Gal4 DNA-binding domain (pDEST-DBD). The resulting plasmids contained an ORF with the AD or DBD fused to the N terminus and were transformed into Y8800 (*MAT***a**) and Y8930 (*MATα*), respectively. Self-activation of the DBD-X and AD-Y was assessed by mating the DBD-X (*MATα*) or AD-Y (*MAT***a**) with yeast strains carrying empty vector expressing only the AD or DBD. After mating, diploids containing both the bait (Gal4-DBD-X) and the prey (Gal4-AD-Y) were isolated, grown overnight in SD-leu-trp medium at 30°C, serially diluted, and then spotted onto SD-leu-trp, SD-leu-trp-his and SD-leu-trp-his + 3AT (0.5 mM and 1 mM) plates. The plates were incubated at 30°C for 3–4 d and imaged on a Canon CanoScan 8800F Scanner.

Raw images

Original data underlying Fig. 3 e, Fig. 5 d, Fig. 6 (c and d), and Fig. S2 e can be downloaded from the Stowers Original Data Repository at https://www.stowers.org/research/publications/libpb-1300.

Online supplemental material

Fig. S1 shows analysis of diploidized *rscΔ* mutants. Fig. S2 shows characterization of SPB defects in *rsc* mutants. Fig. S3 identifies transcriptional targets of RSC and shows a lack of physical interaction between RSC and SPB components. Fig. S4 shows the consequences of depleting Htl1 on ploidy and SPB size and localization. Fig. S5 shows corresponding flow cytometry for samples in Fig. 6. Fig. S6 shows corresponding flow cytometry for samples in Fig. 8 and raw data for Fig. 8 (c and d). Table S1 shows morphological features extracted from analysis in Fig. 2 b. Table S2 shows RNA sequencing data for *rsc* mutants. Table S3 shows SGA data for *rscΔ* mutants. Table S4 lists yeast strains used in this study. Table S5 lists plasmids used in this study. Videos 1–5 contain the image sequences from Fig. 3 d.

References

Afgan, E., D. Baker, M. van den Beek, D. Blankenberg, D. Bouvier, M. Čech, J. Chilton, D. Clements, N. Coraor, C. Eberhard, et al. 2016. The Galaxy platform for accessible, reproducible and collaborative biomedical analyses: 2016 update. *Nucleic Acids Res.* 44(W1):W3–W10. https://doi.org/10.1093/nar/gkw343

Angus-Hill, M.L., A. Schlichter, D. Roberts, H. Erdjument-Bromage, P. Tempst, and B.R. Cairns. 2001. A Rsc3/Rsc30 zinc cluster dimer reveals novel roles for the chromatin remodeler RSC in gene expression and cell cycle control. *Mol. Cell.* 7:741–751. https://doi.org/10.1016/S1097-2765(01)00219-2

Araki, Y., C.K. Lau, H. Maekawa, S.L. Jaspersen, T.H. Giddings Jr., E. Schiebel, and M. Winey. 2006. The *Saccharomyces cerevisiae* spindle pole body (SPB) component Nbp1p is required for SPB membrane insertion and interacts with the integral membrane proteins Ndc1p and Mps2p. *Mol. Biol. Cell.* 17:1959–1970. https://doi.org/10.1091/mbc.e05-07-0668

Avena, J.S., S. Burns, Z. Yu, C.C. Ebmeier, W.M. Old, S.L. Jaspersen, and M. Winey. 2014. Licensing of yeast centrosome duplication requires phosphoregulation of sfi1. *PLoS Genet.* 10:e1004666. https://doi.org/10.1371/journal.pgen.1004666

Badis, G., E.T. Chan, H. van Bakel, L. Pena-Castillo, D. Tillo, K. Tsui, C.D. Carlson, A.J. Gossett, M.J. Hasinoff, C.L. Warren, et al. 2008. A library of yeast transcription factor motifs reveals a widespread function for Rsc3 in targeting nucleosome exclusion at promoters. *Mol. Cell.* 32:878–887. https://doi.org/10.1016/j.molcel.2008.11.020

Baetz, K.K., N.J. Krogan, A. Emili, J. Greenblatt, and P. Hieter. 2004. The ctf13-30/CTF13 genomic haploinsufficiency modifier screen identifies the yeast chromatin remodeling complex RSC, which is required for the establishment of sister chromatid cohesion. *Mol. Cell. Biol.* 24:1232–1244. https://doi.org/10.1128/MCB.24.3.1232-1244.2003

Bellay, J., G. Atluri, T.L. Sing, K. Toufighi, M. Costanzo, P.S.M. Ribeiro, G. Pandey, J. Baller, B. VanderSluis, M. Michaut, et al. 2011. Putting genetic interactions in context through a global modular decomposition. *Genome Res.* 21:1375–1387. https://doi.org/10.1101/gr.117176.110

Bossie, M.A., and P.A. Silver. 1992. Movement of macromolecules between the cytoplasm and the nucleus in yeast. *Curr. Opin. Genet. Dev.* 2:768–774. https://doi.org/10.1016/S0959-437X(05)80137-6

Brachmann, C.B., A. Davies, G.J. Cost, E. Caputo, J. Li, P. Hieter, and J.D. Boeke. 1998. Designer deletion strains derived from *Saccharomyces cerevisiae* S288C: A useful set of strains and plasmids for PCR-mediated gene disruption and other applications. *Yeast.* 14:115–132. https://doi.org/10.1002/(SICI)1097-0061(19980130)14:2%3C115::AID-YEA204%3E3.0.CO;2-2

Burns, S., J.S. Avena, J.R. Unruh, Z. Yu, S.E. Smith, B.D. Slaughter, M. Winey, and S.L. Jaspersen. 2015. Structured illumination with particle averaging reveals novel roles for yeast centrosome components during duplication. *eLife.* 4:1–27. https://doi.org/10.7554/eLife.08586

Cairns, B.R., Y. Lorch, Y. Li, M. Zhang, L. Lacomis, H. Erdjument-Bromage, P. Tempst, J. Du, B. Laurent, and R.D. Kornberg. 1996. RSC, an essential, abundant chromatin-remodeling complex. *Cell.* 87:1249–1260. https://doi.org/10.1016/S0092-8674(00)81820-6

Cairns, B.R., H. Erdjument-Bromage, P. Tempst, F. Winston, and R.D. Kornberg. 1998. Two actin-related proteins are shared functional components of the chromatin-remodeling complexes RSC and SWI/SNF. *Mol. Cell.* 2:639–651. https://doi.org/10.1016/S1097-2765(00)80162-8

Cairns, B.R., A. Schlichter, H. Erdjument-Bromage, P. Tempst, R.D. Kornberg, and F. Winston. 1999. Two functionally distinct forms of the RSC nucleosome-remodeling complex, containing essential AT hook, BAH, and bromodomains. *Mol. Cell.* 4:715–723. https://doi.org/10.1016/S1097-2765(00)80382-2

Campsteijn, C., A.-M.J. Wijnands-Collin, and C. Logie. 2007. Reverse genetic analysis of the yeast RSC chromatin remodeler reveals a role for RSC3 and SNF5 homolog 1 in ploidy maintenance. *PLoS Genet.* 3:e92. https://doi.org/10.1371/journal.pgen.0030092

Cao, Y., B.R. Cairns, R.D. Kornberg, and B.C. Laurent. 1997. Sfh1p, a component of a novel chromatin-remodeling complex, is required for cell cycle progression. *Mol. Cell. Biol.* 17:3323–3334. https://doi.org/10.1128/MCB.17.6.3323

Chambers, A.L., G. Ormerod, S.C. Durley, T.L. Sing, G.W. Brown, N.A. Kent, and J.A. Downs. 2012. The INO80 chromatin remodeling complex prevents polyploidy and maintains normal chromatin structure at centromeres. *Genes Dev.* 26:2590–2603. https://doi.org/10.1101/gad.199976.112

Chen, J., C.J. Smoyer, B.D. Slaughter, J.R. Unruh, and S.L. Jaspersen. 2014. The SUN protein Mps3 controls Ndc1 distribution and function on the nuclear membrane. *J. Cell Biol.* 204:523–539. https://doi.org/10.1083/jcb.201307043

Chial, H.J., T.H. Giddings Jr., E.A. Siewert, M.A. Hoyt, and M. Winey. 1999. Altered dosage of the *Saccharomyces cerevisiae* spindle pole body duplication gene, *NDC1*, leads to aneuploidy and polyploidy. *Proc. Natl. Acad. Sci. USA.* 96:10200–10205. https://doi.org/10.1073/pnas.96.18.10200

Costanzo, M., A. Baryshnikova, J. Bellay, Y. Kim, E.D. Spear, C.S. Sevier, H. Ding, J.L.Y. Koh, K. Toufighi, S. Mostafavi, et al. 2010. The genetic landscape of a cell. *Science.* 327:425–431. https://doi.org/10.1126/science.1180823

Damelin, M., I. Simon, T.I. Moy, B. Wilson, S. Komili, P. Tempst, F.P. Roth, R.A. Young, B.R. Cairns, and P.A. Silver. 2002. The genome-wide localization of Rsc9, a component of the RSC chromatin-remodeling complex, changes in response to stress. *Mol. Cell.* 9:563–573. https://doi.org/10.1016/S1097-2765(02)00475-6

Davoli, T., and T. de Lange. 2011. The causes and consequences of polyploidy in normal development and cancer. *Annu. Rev. Cell Dev. Biol.* 27:585–610. https://doi.org/10.1146/annurev-cellbio-092910-154234

Desai, P., N. Guha, L. Galdieri, S. Hadi, and A. Vancura. 2009. Plc1p is required for proper chromatin structure and activity of the kinetochore in *Saccharomyces cerevisiae* by facilitating recruitment of the RSC complex. *Mol. Genet. Genomics.* 281:511–523. https://doi.org/10.1007/s00438-009-0427-9

Dion, B., and G.W. Brown. 2009. Comparative genome hybridization on tiling microarrays to detect aneuploidies in yeast. *Methods Mol. Biol.* 548:1–18. https://doi.org/10.1007/978-1-59745-540-4_1

Elserafy, M., M. Šarić, A. Neuner, T.-C. Lin, W. Zhang, C. Seybold, L. Sivashanmugam, and E. Schiebel. 2014. Molecular mechanisms that restrict yeast centrosome duplication to one event per cell cycle. *Curr. Biol.* 24:1456–1466. https://doi.org/10.1016/j.cub.2014.05.032

Fields, S., and O. Song. 1989. A novel genetic system to detect protein-protein interactions. *Nature.* 340:245–246. https://doi.org/10.1038/340245a0

Friederichs, J.M., S. Ghosh, C.J. Smoyer, S. McCroskey, B.D. Miller, K.J. Weaver, K.M. Delventhal, J. Unruh, B.D. Slaughter, and S.L. Jaspersen. 2011. The SUN protein Mps3 is required for spindle pole body insertion into the nuclear membrane and nuclear envelope homeostasis. *PLoS Genet.* 7:e1002365. https://doi.org/10.1371/journal.pgen.1002365

Gerstein, A.C., H.J.E. Chun, A. Grant, and S.P. Otto. 2006. Genomic convergence toward diploidy in *Saccharomyces cerevisiae*. *PLoS Genet.* 2:e145. https://doi.org/10.1371/journal.pgen.0020145

Giaever, G., and C. Nislow. 2014. The yeast deletion collection: A decade of functional genomics. *Genetics.* 197:451–465. https://doi.org/10.1534/genetics.114.161620

Harrison, B.D., J. Hashemi, M. Bibi, R. Pulver, D. Bavli, Y. Nahmias, M. Wellington, G. Sapiro, and J. Berman. 2014. A tetraploid intermediate precedes aneuploid formation in yeasts exposed to fluconazole. *PLoS Biol.* 12:e1001815. https://doi.org/10.1371/journal.pbio.1001815

Hsu, J.M., J. Huang, P.B. Meluh, and B.C. Laurent. 2003. The yeast RSC chromatin-remodeling complex is required for kinetochore function in chromosome segregation. *Mol. Cell. Biol.* 23:3202–3215. https://doi.org/10.1128/MCB.23.9.3202-3215.2003

Hu, Y., A. Rolfs, B. Bhullar, T.V.S. Murthy, C. Zhu, M.F. Berger, A.A. Camargo, F. Kelley, S. McCarron, D. Jepson, et al. 2007. Approaching a complete repository of sequence-verified protein-encoding clones for *Saccharomyces cerevisiae*. *Genome Res.* 17:536–543. https://doi.org/10.1101/gr.6037607

Huang, J., J.-M. Hsu, and B.C. Laurent. 2004. The RSC nucleosome-remodeling complex is required for Cohesin's association with chromosome arms. *Mol. Cell.* 13:739–750. https://doi.org/10.1016/S1097-2765(04)00103-0

Huh, W.K., J.V. Falvo, L.C. Gerke, A.S. Carroll, R.W. Howson, J.S. Weissman, and E.K. O'Shea. 2003. Global analysis of protein localization in budding yeast. *Nature.* 425:686–691. https://doi.org/10.1038/nature02026

Imamura, Y., F. Yu, M. Nakamura, Y. Chihara, K. Okane, M. Sato, M. Kanai, R. Hamada, M. Ueno, M. Yukawa, and E. Tsuchiya. 2015. RSC chromatin-remodeling complex is important for mitochondrial function in *Saccharomyces cerevisiae*. *PLoS One.* 10:e0130397. https://doi.org/10.1371/journal.pone.0130397

Isakoff, M.S., C.G. Sansam, P. Tamayo, A. Subramanian, J.A. Evans, C.M. Fillmore, X. Wang, J.A. Biegel, S.L. Pomeroy, J.P. Mesirov, and C.W. Roberts. 2005. Inactivation of the Snf5 tumor suppressor stimulates cell cycle progression and cooperates with p53 loss in oncogenic transformation. *Proc. Natl. Acad. Sci. USA.* 102:17745–17750. https://doi.org/10.1073/pnas.0509014102

Jaspersen, S.L., and M. Winey. 2004. The budding yeast spindle pole body: Structure, duplication, and function. *Annu. Rev. Cell Dev. Biol.* 20:1–28. https://doi.org/10.1146/annurev.cellbio.20.022003.114106

Jaspersen, S.L., T.H. Giddings Jr., and M. Winey. 2002. Mps3p is a novel component of the yeast spindle pole body that interacts with the yeast centrin homologue Cdc31p. *J. Cell Biol.* 159:945–956. https://doi.org/10.1083/jcb.200208169

Katta, S.S., J. Chen, J.M. Gardner, J.M. Friederichs, S.E. Smith, M. Gogol, J.R. Unruh, B.D. Slaughter, and S.L. Jaspersen. 2015. Sec66-dependent regulation of yeast spindle-pole body duplication through Pom152. *Genetics.* 201:1479–1495. https://doi.org/10.1534/genetics.115.178012

Kupke, T., L. Di Cecco, H.-M. Müller, A. Neuner, F. Adolf, F. Wieland, W. Nickel, and E. Schiebel. 2011. Targeting of Nbp1 to the inner nuclear membrane is essential for spindle pole body duplication. *EMBO J.* 30:3337–3352. https://doi.org/10.1038/emboj.2011.242

Lambert, J.-P., J. Fillingham, M. Siahbazi, J. Greenblatt, K. Baetz, and D. Figeys. 2010. Defining the budding yeast chromatin-associated interactome. *Mol. Syst. Biol.* 6:448. https://doi.org/10.1038/msb.2010.104

Lanzuolo, C., S. Ederle, A. Pollice, F. Russo, A. Storlazzi, and J.F. Pulitzer. 2001. The *HTL1* gene (YCR020W-b) of *Saccharomyces cerevisiae* is necessary for growth at 37°C, and for the conservation of chromosome stability and fertility. *Yeast.* 18:1317–1330. https://doi.org/10.1002/yea.778

Lau, C.K., T.H. Giddings Jr., and M. Winey. 2004. A novel allele of Saccharomyces cerevisiae *NDC1* reveals a potential role for the spindle pole body component Ndc1p in nuclear pore assembly. *Eukaryot. Cell.* 3:447–458. https://doi.org/10.1128/EC.3.2.447-458.2004

Laurent, B.C., X. Yang, and M. Carlson. 1992. An essential *Saccharomyces cerevisiae* gene homologous to *SNF2* encodes a helicase-related protein in a new family. *Mol. Cell. Biol.* 12:1893–1902. https://doi.org/10.1128/MCB.12.4.1893

Lengefeld, J., M. Hotz, M. Rollins, K. Baetz, and Y. Barral. 2017. Budding yeast Wee1 distinguishes spindle pole bodies to guide their pattern of age-dependent segregation. *Nat. Cell Biol.* 19:941–951. https://doi.org/10.1038/ncb3576

Liefshitz, B., and M. Kupiec. 2011. Roles of RSC, Rad59, and cohesin in double-strand break repair. *Mol. Cell. Biol.* 31:3921–3923. https://doi.org/10.1128/MCB.05974-11

Lopez-Serra, L., G. Kelly, H. Patel, A. Stewart, and F. Uhlmann. 2014. The Scc2-Scc4 complex acts in sister chromatid cohesion and transcriptional

regulation by maintaining nucleosome-free regions. *Nat. Genet.* 46:1147–1151. https://doi.org/10.1038/ng.3080

Magtanong, L., C.H. Ho, S.L. Barker, W. Jiao, A. Baryshnikova, S. Bahr, A.M. Smith, L.E. Heisler, J.S. Choy, E. Kuzmin, et al. 2011. Dosage suppression genetic interaction networks enhance functional wiring diagrams of the cell. *Nat. Biotechnol.* 29:505–511. https://doi.org/10.1038/nbt.1855

Marguerat, S., and J. Bähler. 2012. Coordinating genome expression with cell size. *Trends Genet.* 28:560–565. https://doi.org/10.1016/j.tig.2012.07.003

McDonald, K. 1999. High-pressure freezing for preservation of high resolution fine structure and antigenicity for immunolabeling. *Methods Mol. Biol.* 117:79–97.

Meseroll, R.A., and O. Cohen-Fix. 2016. The malleable nature of the budding yeast nuclear envelope: Flares, fusion, and fenestrations. *J. Cell. Physiol.* 231:2353–2360. https://doi.org/10.1002/jcp.25355

Ng, H.H., F. Robert, R.A. Young, and K. Struhl. 2002. Genome-wide location and regulated recruitment of the RSC nucleosome-remodeling complex. *Genes Dev.* 16:806–819. https://doi.org/10.1101/gad.978902

Ohya, Y., J. Sese, M. Yukawa, F. Sano, Y. Nakatani, T.L. Saito, A. Saka, T. Fukuda, S. Ishihara, S. Oka, et al. 2005. High-dimensional and large-scale phenotyping of yeast mutants. *Proc. Natl. Acad. Sci. USA.* 102:19015–19020. https://doi.org/10.1073/pnas.0509436102

Ohya, Y., Y. Kimori, H. Okada, and S. Ohnuki. 2015. Single-cell phenomics in budding yeast. *Mol. Biol. Cell.* 26:3920–3925. https://doi.org/10.1091/mbc.e15-07-0466

Okagaki, L.H., and K. Nielsen. 2012. Titan cells confer protection from phagocytosis in Cryptococcus neoformans infections. *Eukaryot. Cell.* 11:820–826. https://doi.org/10.1128/EC.00121-12

Onischenko, E., L.H. Stanton, A.S. Madrid, T. Kieselbach, and K. Weis. 2009. Role of the Ndc1 interaction network in yeast nuclear pore complex assembly and maintenance. *J. Cell Biol.* 185:475–491. https://doi.org/10.1083/jcb.200810030

Otsu, N. 1979. A threshold selection method from gray-level histograms. *IEEE Trans. Syst. Man Cybern.* 9:62–66. https://doi.org/10.1109/TSMC.1979.4310076

Otto, S.P. 2007. The evolutionary consequences of polyploidy. *Cell.* 131:452–462. https://doi.org/10.1016/j.cell.2007.10.022

Oum, J.-H., C. Seong, Y. Kwon, J.-H. Ji, A. Sid, S. Ramakrishnan, G. Ira, A. Malkova, P. Sung, S.E. Lee, and E.Y. Shim. 2011. RSC facilitates Rad59-dependent homologous recombination between sister chromatids by promoting cohesin loading at DNA double-strand breaks. *Mol. Cell. Biol.* 31:3924–3937. https://doi.org/10.1128/MCB.01269-10

Parnell, T.J., J.T. Huff, and B.R. Cairns. 2008. RSC regulates nucleosome positioning at Pol II genes and density at Pol III genes. *EMBO J.* 27:100–110. https://doi.org/10.1038/sj.emboj.7601946

Ptak, C., A.M. Anderson, R.J. Scott, D. Van de Vosse, R.S. Rogers, Y. Sydorskyy, J.D. Aitchison, and R.W. Wozniak. 2009. A role for the karyopherin Kap123p in microtubule stability. *Traffic.* 10:1619–1634. https://doi.org/10.1111/j.1600-0854.2009.00978.x

Reimand, J., T. Arak, P. Adler, L. Kolberg, S. Reisberg, H. Peterson, and J. Vilo. 2016. g:Profiler-a web server for functional interpretation of gene lists (2016 update). *Nucleic Acids Res.* 44(W1):W83–W89. https://doi.org/10.1093/nar/gkw199

Romeo, M.J., M.L. Angus-Hill, A.K. Sobering, Y. Kamada, B.R. Cairns, and D.E. Levin. 2002. *HTL1* encodes a novel factor that interacts with the RSC chromatin remodeling complex in *Saccharomyces cerevisiae. Mol. Cell. Biol.* 22:8165–8174. https://doi.org/10.1128/MCB.22.23.8165-8174.2002

Rüthnick, D., A. Neuner, F. Dietrich, D. Kirrmaier, U. Engel, and M. Knop. 2017. Characterization of spindle pole body duplication reveals a regulatory role for nuclear pore complexes. *J. Cell Biol.* 216:2425–2442. https://doi.org/10.1083/jcb.201612129

Sanders, S.L., J. Jennings, A. Canutescu, A.J. Link, and P.A. Weil. 2002. Proteomics of the eukaryotic transcription machinery: Identification of proteins associated with components of yeast TFIID by multidimensional mass spectrometry. *Mol. Cell. Biol.* 22:4723–4738. https://doi.org/10.1128/MCB.22.13.4723-4738.2002

Schild, D., H.N. Ananthaswamy, and R.K. Mortimer. 1981. An endomitotic effect of a cell cycle mutation of *Saccharomyces cerevisiae. Genetics.* 97:551–562.

Schramm, C., S. Elliott, A. Shevchenko, and E. Schiebel. 2000. The Bbp1p-Mps2p complex connects the SPB to the nuclear envelope and is essential for SPB duplication. *EMBO J.* 19:421–433. https://doi.org/10.1093/emboj/19.3.421

Sezen, B. 2015. Reduction of *Saccharomyces cerevisiae* Pom34 protein level by SESA network is related to membrane lipid composition. *FEMS Yeast Res.* 15:1–7. https://doi.org/10.1093/femsyr/fov089

Sezen, B., M. Seedorf, and E. Schiebel. 2009. The SESA network links duplication of the yeast centrosome with the protein translation machinery. *Genes Dev.* 23:1559–1570. https://doi.org/10.1101/gad.524209

Sherman, F. 2002. Getting started with yeast. *Methods Enzymol.* 350:3–41. https://doi.org/10.1016/S0076-6879(02)50954-X

Sillibourne, J.E., B. Delaval, S. Redick, M. Sinha, and S.J. Doxsey. 2007. Chromatin remodeling proteins interact with pericentrin to regulate centrosome integrity. *Mol. Biol. Cell.* 18:3667–3680. https://doi.org/10.1091/mbc.e06-07-0604

Sinha, M., and C.L. Peterson. 2009. Chromatin dynamics during repair of chromosomal DNA double-strand breaks. *Epigenomics.* 1:371–385. https://doi.org/10.2217/epi.09.22

Storey, J.D. 2002. A direct approach to false discovery rates. *J. R. Stat. Soc. Series B Stat. Methodol.* 64:479–498. https://doi.org/10.1111/1467-9868.00346

St Pierre, R., and C. Kadoch. 2017. Mammalian SWI/SNF complexes in cancer: Emerging therapeutic opportunities. *Curr. Opin. Genet. Dev.* 42:56–67. https://doi.org/10.1016/j.gde.2017.02.004

Sung, M.K., and W.K. Huh. 2007. Bimolecular fluorescence complementation analysis system for in vivo detection of protein-protein interaction in *Saccharomyces cerevisiae. Yeast.* 24:767–775. https://doi.org/10.1002/yea.1504

Titus, L.C., T.R. Dawson, D.J. Rexer, K.J. Ryan, and S.R. Wente. 2010. Members of the RSC chromatin-remodeling complex are required for maintaining proper nuclear envelope structure and pore complex localization. *Mol. Biol. Cell.* 21:1072–1087. https://doi.org/10.1091/mbc.e09-07-0615

Tong, A.H.Y., M. Evangelista, A.B. Parsons, H. Xu, G.D. Bader, N. Pagé, M. Robinson, S. Raghibizadeh, C.W.V. Hogue, H. Bussey, et al. 2001. Systematic genetic analysis with ordered arrays of yeast deletion mutants. *Science.* 294:2364–2368. https://doi.org/10.1126/science.1065810

Trapnell, C., A. Roberts, L. Goff, G. Pertea, D. Kim, D.R. Kelley, H. Pimentel, S.L. Salzberg, J.L. Rinn, and L. Pachter. 2012. Differential gene and transcript expression analysis of RNA-seq experiments with TopHat and Cufflinks. *Nat. Protoc.* 7:562–578. https://doi.org/10.1038/nprot.2012.016

Tsuchiya, E., T. Hosotani, and T. Miyakawa. 1998. A mutation in *NPS1/STH1*, an essential gene encoding a component of a novel chromatin-remodeling complex RSC, alters the chromatin structure of *Saccharomyces cerevisiae* centromeres. *Nucleic Acids Res.* 26:3286–3292. https://doi.org/10.1093/nar/26.13.3286

Ungar, L., N. Yosef, Y. Sela, R. Sharan, E. Ruppin, and M. Kupiec. 2009. A genome-wide screen for essential yeast genes that affect telomere length maintenance. *Nucleic Acids Res.* 37:3840–3849. https://doi.org/10.1093/nar/gkp259

Van de Vosse, D.W., Y. Wan, D.L. Lapetina, W.-M. Chen, J.-H. Chiang, J.D. Aitchison, and R.W. Wozniak. 2013. A role for the nucleoporin Nup170p in chromatin structure and gene silencing. *Cell.* 152:969–983. https://doi.org/10.1016/j.cell.2013.01.049

Verdaasdonk, J.S., R. Gardner, A.D. Stephens, E. Yeh, and K. Bloom. 2012. Tension-dependent nucleosome remodeling at the pericentromere in yeast. *Mol. Biol. Cell.* 23:2560–2570. https://doi.org/10.1091/mbc.e11-07-0651

Vries, R.G.J., V. Bezrookove, L.M.P. Zuijderduijn, S.K. Kia, A. Houweling, I. Oruetxebarria, A.K. Raap, and C.P. Verrijzer. 2005. Cancer-associated mutations in chromatin remodeler hSNF5 promote chromosomal instability by compromising the mitotic checkpoint. *Genes Dev.* 19:665–670. https://doi.org/10.1101/gad.335805

Wang, S.L., and M.Y. Cheng. 2012. The defects in cell wall integrity and G2-M transition of the Δhtl1 mutant are interconnected. *Yeast.* 29:45–57. https://doi.org/10.1002/yea.1916

Watanabe, M., D. Watanabe, S. Nogami, S. Morishita, and Y. Ohya. 2009. Comprehensive and quantitative analysis of yeast deletion mutants defective in apical and isotropic bud growth. *Curr. Genet.* 55:365–380. https://doi.org/10.1007/s00294-009-0251-0

Winey, M., and K. Bloom. 2012. Mitotic spindle form and function. *Genetics.* 190:1197–1224. https://doi.org/10.1534/genetics.111.128710

Winey, M., L. Goetsch, P. Baum, and B. Byers. 1991. *MPS1* and *MPS2*: Novel yeast genes defining distinct steps of spindle pole body duplication. *J. Cell Biol.* 114:745–754. https://doi.org/10.1083/jcb.114.4.745

Winey, M., M.A. Hoyt, C. Chan, L. Goetsch, D. Botstein, and B. Byers. 1993. NDC1: A nuclear periphery component required for yeast spindle pole body duplication. *J. Cell Biol.* 122:743–751. https://doi.org/10.1083/jcb.122.4.743

Witkin, K.L., J.M. Friederichs, O. Cohen-Fix, and S.L. Jaspersen. 2010. Changes in the nuclear envelope environment affect spindle pole body duplication in *Saccharomyces cerevisiae*. *Genetics*. 186:867–883. https://doi.org/10.1534/genetics.110.119149

Witkin, K.L., Y. Chong, S. Shao, M.T. Webster, S. Lahiri, A.D. Walters, B. Lee, J.L.Y. Koh, W.A. Prinz, B.J. Andrews, and O. Cohen-Fix. 2012. The budding yeast nuclear envelope adjacent to the nucleolus serves as a membrane sink during mitotic delay. *Curr. Biol.* 22:1128–1133. https://doi.org/10.1016/j.cub.2012.04.022

Wong, M.C.V.L., S.R.S. Scott-Drew, M.J. Hayes, P.J. Howard, and J.A.H. Murray. 2002. RSC2, encoding a component of the RSC nucleosome remodeling complex, is essential for 2 microm plasmid maintenance in *Saccharomyces cerevisiae*. *Mol. Cell. Biol.* 22:4218–4229. https://doi.org/10.1128/MCB.22.12.4218-4229.2002

Xue, Y., J.C. Canman, C.S. Lee, Z. Nie, D. Yang, G.T. Moreno, M.K. Young, E.D. Salmon, and W. Wang. 2000. The human SWI/SNF-B chromatin-remodeling complex is related to yeast rsc and localizes at kinetochores of mitotic chromosomes. *Proc. Natl. Acad. Sci. USA.* 97:13015–13020. https://doi.org/10.1073/pnas.240208597

Yu, L., L. Peña Castillo, S. Mnaimneh, T.R. Hughes, and G.W. Brown. 2006. A survey of essential gene function in the yeast cell division cycle. *Mol. Biol. Cell.* 17:4736–4747. https://doi.org/10.1091/mbc.e06-04-0368

Zaragoza, O., R. García-Rodas, J.D. Nosanchuk, M. Cuenca-Estrella, J.L. Rodríguez-Tudela, and A. Casadevall. 2010. Fungal cell gigantism during mammalian infection. *PLoS Pathog.* 6:e1000945. https://doi.org/10.1371/journal.ppat.1000945